*Chemical Senses*, 2023, **48**, 1–18
https://doi.org/10.1093/chemse/bjad042
Advance access publication 18 October 2023
**Original Article**

Original Article

# Oral thermal processing in the gustatory cortex of awake mice

**Cecilia G. Bouaichi[1,†], Katherine E. Odegaard[1,†], Camden Neese[1], Roberto Vincis[2,*]**

[1]Department of Biological Science and Programs in Neuroscience, Cell and Molecular Biology, and Biophysics, Florida State University, Tallahassee, FL, United States
[2]Department of Biological Science and Programs in Neuroscience, Molecular Biophysics and Cell and Molecular Biology, Florida State University, Tallahassee, FL, United States

[†]These authors contributed equally to this work.
[*]Corresponding author: Department of Biological Science and Programs in Neuroscience, Molecular Biophysics and Cell and Molecular Biology, Florida State University, BRF 107 Chieftan way, Tallahassee, FL, USA. Email: rvincis@fsu.edu

Oral temperature is a sensory cue relevant to food preference and nutrition. To understand how orally sourced thermal inputs are represented in the gustatory cortex (GC), we recorded neural responses from the GC of male and female mice presented with deionized water at different innocuous temperatures (14 °C, 25 °C, and 36 °C) and taste stimuli (room temperature). Our results demonstrate that GC neurons encode orally sourced thermal information in the absence of classical taste qualities at the single neuron and population levels, as confirmed through additional experiments comparing GC neuron responses to water and artificial saliva. Analysis of thermal-evoked responses showed broadly tuned neurons that responded to temperature in a mostly monotonic manner. Spatial location may play a minor role regarding thermosensory activity; aside from the most ventral GC, neurons reliably responded to and encoded thermal information across the dorso-ventral and antero-postero cortical axes. Additional analysis revealed that more than half of the GC neurons that encoded chemosensory taste stimuli also accurately discriminated thermal information, providing additional evidence of the GC's involvement in processing thermosensory information important for ingestive behaviors. In terms of convergence, we found that GC neurons encoding information about both taste and temperature were broadly tuned and carried more information than taste-selective-only neurons; both groups encoded similar information about the palatability of stimuli. Altogether, our data reveal new details of the cortical code for the mammalian oral thermosensory system in behaving mice and pave the way for future investigations on GC functions and operational principles with respect to thermogustation.

**Key words:** oral, gustatory, thermal, cortex, flavor, eating.

## Introduction

The consumption of food and beverages is highly dependent on the initial sensation and the response it evokes (Dotson et al. 2012; Schier and Spector 2019). This sensation arises within the mouth and involves the integration of intraoral gustatory, olfactory, and somatosensory cues in a single percept called flavor (Kemp and Beauchamp 1994; Small 2012). In the past decades, many electrophysiological studies in behaving rodents have investigated the physiological correlates of one of these intraoral sensory components—taste—which originates when chemical compounds stimulate specialized chemoreceptors within the oral cavity (Spector and Travers 2005; Vincis and Fontanini 2019). Using gustatory stimuli at a fixed temperature, these studies made clear that taste information is processed through neural computations that occur in interconnected brain areas that include the gustatory cortex (GC), the primary cortical area responsible for processing taste information (Katz et al. 2001; Stapleton et al. 2006; Roussin et al. 2012; Jezzini et al. 2013; Samuelsen et al. 2013; Liu and Fontanini 2015; Levitan et al. 2019; Bouaichi and Vincis 2020). In addition, these studies have indicated that GC neurons respond to compounds representing different taste qualities and their hedonic value with time-varying patterns of activity (Katz et al. 2001; Jezzini et al. 2013; Arieli et al. 2020; Bouaichi and Vincis 2020; Neese et al. 2022) and play a role in driving taste-related decisions (Vincis and Fontanini 2016b; Mukherjee et al. 2019; Vincis et al. 2020).

However, a growing body of experimental work indicates that neurons in the GC are also capable of responding to non-gustatory components of intraoral stimuli (De Araujo et al. 2003; Small et al. 2004; Stapleton et al. 2006; Rudenga et al. 2010; Maier 2017; Samuelsen and Fontanini 2017; Bouaichi and Vincis 2020; Samuelsen and Vincis 2021), including temperature—a salient feature of the sensory properties of foods and beverages. Different studies in humans and primates (Cerf-Ducastel et al. 2001; Verhagen et al. 2004; Guest et al. 2007), as well as pioneering works in anesthetized rats (Yamamoto et al. 1981; Kosar et al. 1986), have indicated that changes in oral temperature seem to modulate activity in GC neurons. While these data implicate the GC as a potential key cortical region for the integration of taste and thermal orosensory inputs, they stop short of supplying a fine-grained analysis of the GC's neural responses, and many questions

Editorial Decision 13 October 2023.

remain. Here, using extracellular recording (tetrodes and silicon-based probes), we aim to provide a complete neurophysiological assessment of how thermal orosensory inputs shape GC activity in alert mice. Specifically, this study is designed to assess (i) whether and how neurons in the GC of actively licking mice are modulated by changes in the temperature of a chemically inert drinking solution, (ii) the spatial organization of oral thermal-related information across the GC, and (iii) the extent to which GC neurons respond to both oral thermal and taste information.

## Materials and methods

### Data acquisition

The experiments in this study were performed on 34 wild-type C57BL/6J adult mice (10 to 20 weeks old; 16 males and 18 females) that were purchased from The Jackson Laboratory (Bar Harbor, ME). Upon arrival at the animal facility, animals were housed on a 12-h/12-h light–dark cycle and had ad libitum access to food and water. Experiments and training were performed during the light portion of the cycle. All experiments were reviewed and approved by the Florida State University Institutional Animal Care and Use Committee under protocol PROTO202100006.

### Surgery

All animals were anesthetized with an intraperitoneal injection of a cocktail of ketamine (25 mg/kg) and dexmedetomidine (0.25 mg/kg). The depth of anesthesia was monitored regularly via visual inspection of breathing rate, whisker reflexes, and tail reflex. Anesthesia was supplemented by ¼ of the original dose of ketamine as needed throughout the surgery. A heating pad (DC temperature control system, FHC, Bowdoin, ME) was used to maintain body temperature at 35 °C. At the start of surgery, mice were also dosed with dexamethasone (0.4 mg/kg, intramuscular) and bupivacaine HCl (2%, subcutaneous). In addition, lactate solutions were administered every 0.5 h during surgery at volumes of 0.5 ml. Once a surgical plane of anesthesia was achieved, the animal's head was shaved, cleaned, and disinfected (with iodine solution and 70% alcohol) before being fixed on a stereotaxic holder. To record extracellular activity, mice were implanted with either a custom-made movable bundle of 8 tetrodes [the same used and described in Bouaichi and Vincis (2020), Vincis et al. (2020), Neese et al. (2022); $n$ = 28 mice] or with one of the 2 types of chronic and movable silicon probes mounted on a nanodrive shuttle (Cambridge Neurotech, Cambridge, UK). One probe (H5, Cambridge Neurotech; $n$ = 4 mice) had a single shank with 64 electrodes (organized in 2 adjacent rows spaced 22.5 µm apart) evenly spaced at 25-µm intervals; the other (P1, Cambridge Neurotech; $n$ = 2 mice) had 4 shanks separated by 250 µm, where each shank had 16 electrodes (organized in 2 adjacent rows spaced 22.5 µm apart) evenly spaced with 25-µm intervals. Craniotomies were opened above the left GC for implanting tetrodes and probes and above the visual cortex for implanting ground wires (A-M system, Sequim, WA, Cat. No. 781000). Tetrode bundles, the H5 probes, and the anterior shank of the P1 probes were implanted at AP: +1.2 mm and ML: +3.5 mm (relative to bregma) and were slowly lowered above GC (1.5 mm below the cortical surface). Movable bundles and P1 probes were further lowered 300 µm before the first day of the control session recording. H5 probes were further lowered 1200 µm before the first day of the control session recording. Tetrodes or probes and a head screw (for the purpose of head restraint) were cemented to the skull with dental acrylic. Before implantation, tetrode wires and the tips of the silicon probes were coated with a lipophilic fluorescent dye (DiI; Sigma-Aldrich, St. Louis, MO), allowing us to visualize tetrode and probe locations at the end of each experiment. Animals were allowed to recover for a minimum of 7 days before the water restriction regimen and training began. Voltage signals from the tetrodes and probes were acquired, digitized, and band-pass filtered with the Plexon OmniPlex system (Plexon, Dallas, TX) (sampling rate: 40 kHz). The time stamps of task events (licking and stimulus delivery) were collected simultaneously through a MATLAB (MathWorks, Natick, MA)-based behavioral acquisition system (BPOD, Sanworks, Rochester, NY) synchronized with the OmniPlex system.

### Experimental design and statistical analysis

#### Behavioral apparatus and training

One week before training began, mice were mildly water restricted (1.5 ml/day) and maintained at or above 85% of their pre-surgical weight. One week after the start of the water restriction regimen, mice were habituated to be head restrained for short (5 min) daily sessions that gradually progressed (over days) toward longer sessions. During restraint, the body of the mouse was covered with a semicircular opaque plastic shelter to constrain the animal's body movements without stressful constriction (Fig. 1A). The fluid delivery system, licking detection, and behavioral paradigm have been described in detail in previous studies from our group (Bouaichi and Vincis 2020; Neese et al. 2022). Following the habituation to restraint, mice were trained with a behavioral task in which the mice learned to lick a dry spout 6 times to trigger the delivery of the small water drop. Fluid was delivered via gravity by computer-controlled 12 V solenoid valves (Lee Company, Westbrook, CT) calibrated daily to deliver 3 µl from a licking spout (Bouaichi and Vincis 2020; Neese et al. 2022). A peltier block device (ALA Scientific, Farmingdale, NY, or custom-made by FSU Machine Shop) located close to the tip of the licking spout was used to heat or cool the water to a specific temperature. The licking spout was made of short polyamide tubing (ID 0.03, MicroLumen, Oldsmar, FL) exiting the peltier block. The peltier can be heated or cooled to various temperatures between 0 °C and 50 °C by altering the polarity and the magnitude of DC current provided by a central amplifier. These alterations then led to the heating or cooling of an aluminum block, through which the licking tube passed. To calibrate the temperature of the drinking solution, a thermocouple probe was placed at the exit of the licking spout, and the equipment was considered calibrated when the thermocouple reliably read the desired value of fluid temperature. Therefore, the setting of the temperature (with the associated polarity and value of the DC current) on the central amplifier was based upon the temperature of the fluid exiting the licking spout and not the one within the peltier block.

During the habituation and recording sessions (see below for more details), mice received a single 3 µl droplet of deionized water (Barnstead/Thermolyne Nanopure lab water system, Ramsey, MN) at one of the 3 temperatures (14 °C, 25 °C, or 36 °C). These temperatures were chosen for 3 main reasons: (i) they are outside the range of overt noxious thermal stimuli

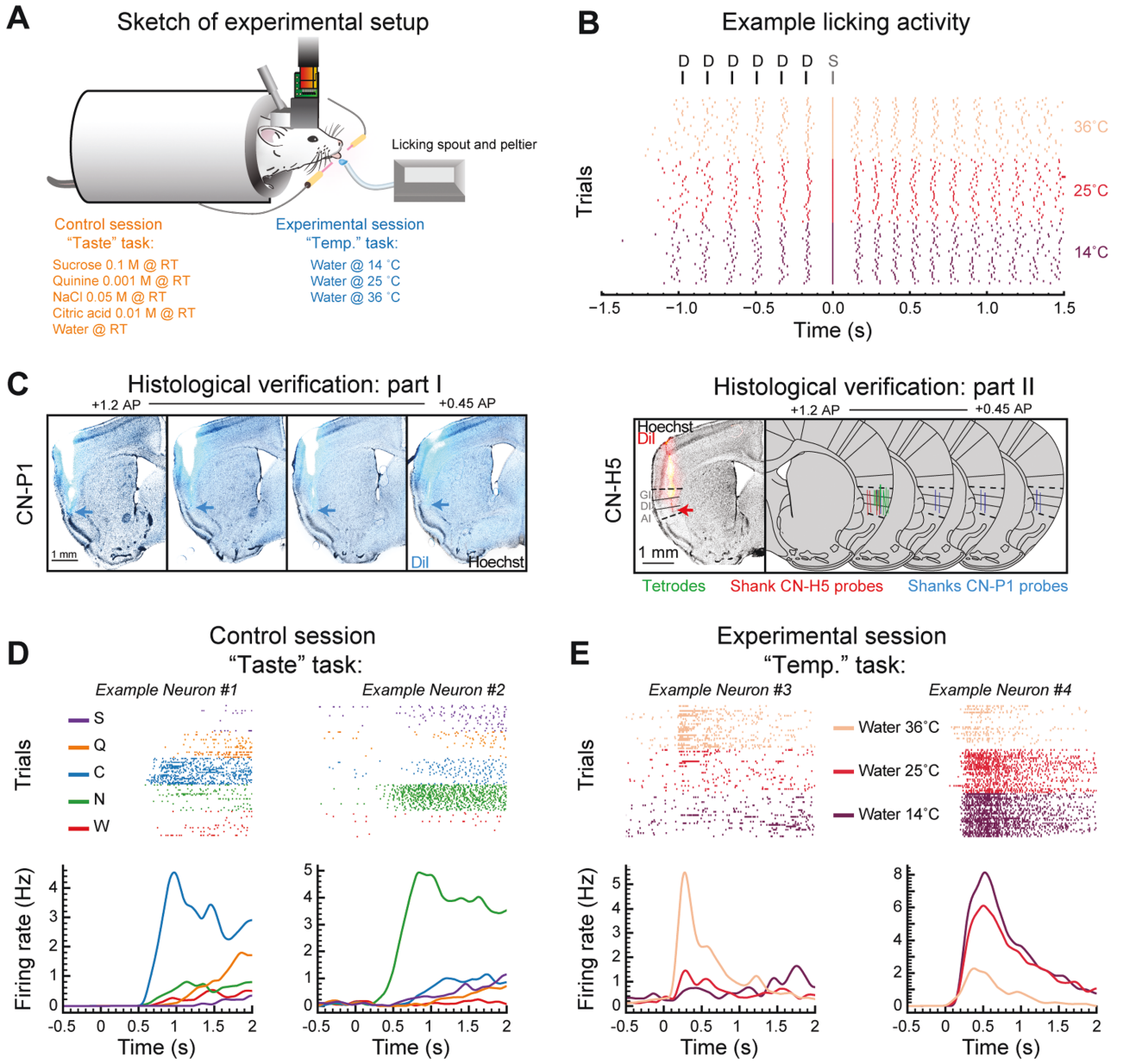


**Fig. 1.** Oral thermal responses in the mouse GC. (A) Schematic showing the recording setup and a head-restrained mouse licking a spout to obtain oral stimuli for 2 different conditions: the control and experimental sessions (see Materials and Methods). (B) *Top*—diagram of the taste delivery paradigm: oral stimuli (S) are delivered after 6 consecutive dry licks (D) to the spout; *bottom*—raster plot of licking activity during one experimental session: each line represents an individual lick; trials pertaining to water at different temperature are grouped together and color-coded. Water delivery occurs at time 0 s. (C) Example of histological sections showing the tracks (cyan) of the 4 shanks of the CN-P1 probe in the GC. Cyan arrows point to the tip of the probe. Scale bar is 1 mm. On the right, there is an example of one histological section showing a CN-H5 probe track (red) in the GC. Red arrow points to the tip of the probe. On the far right, there is a schematic of the summary of the tetrode and probe tracks from the 16 mice whose data are analyzed in Figs. 1–5. Scale bar is 1 mm. (D) Raster plots and PSTHs of 2 representative GC neurons recorded during the control session showing taste responses. Trials pertaining to different tastants are grouped together (in the raster plots) and color-coded (both in the raster plots and PSTHs), with sucrose (S) in purple, quinine (Q) in orange, NaCl (N) in green, citric acid (C) in blue, and water (W) in red. (E) Raster plots and PSTHs of 2 representative GC neurons recorded during the experimental session showing oral thermal responses. Trials pertaining to water at different temperatures are grouped together (in the raster plots) and color-coded (both in the raster plots and PSTHs).

(Suzuki et al. 2003; Allchorne et al. 2005), allowing the animal to be engaged in the task and actively lick for a substantial number of trials (enabling proper statistical analysis of neural data); (ii) they provide compatibility to behavioral studies in rats that investigated the role of water temperature on intake and preference (Torregrossa et al. 2012; Kay et al. 2020); (iii) they represent a broad range of rewarding qualities in water-deprived rats—with colder stimuli being perceived as more rewarding (Torregrossa et al. 2012). To separate neural activity evoked by the oral stimuli from the neural correlates of sensory and motor aspects of licking, we (i) trained the mice to receive each oral stimulus, (ii) trained the mice for up to 2 weeks before recording, allowing for familiarization with the different stimuli, and (iii) did not analyze any imaging or electrophysiological recording session if the licking pattern evoked by each oral stimulus was not similar across

at least a 1.5-s temporal window (Fig. 1B), as defined by a Kruskal–Wallis test. As a result, the neural response evoked by the tastants were compared with the response elicited by licking the dry spout before stimulus delivery. This additional requirement also served to ensure that neural activity evoked by the distinct oral stimuli would not be impacted by differences in stimulus-evoked licking variables. Water–temperature pairings were presented in a block design, with 10 trials for each block and at least 6 blocks per session. For the electrophysiology experiments, we relied not only on stereotaxic coordinates and post hoc evaluation of probe tracks for the successful location of the GC (see Fig. 1C) but also on physiological mapping. To this end, we used the "control session" to record the neural activity evoked by different taste qualities and water presented at room temperature (~22 °C). After this recording session, single neuron spiking activity was analyzed. In the case in which taste-responsive neurons were detected, we proceeded with recording GC neurons while mice performed exclusively the "experimental session" for up to 3 daily sessions. Otherwise, the animals were removed from the study ($n$ = 2). At the end of each experimental session, tetrodes and P1 probes were further lowered in order to sample new GC neuron ensembles (up to 3 recording sessions per mouse). For recording sessions with tetrodes, bundles were lowered ~100 µm after recording each experimental session; for recording sessions with P1 probes, they were lowered 200 µm after recording each experimental session. For recording sessions with H5 probes, we analyzed only the neural recording obtained during one experimental session. In addition to deionized water presented at the selected temperatures mentioned above, the other stimuli used throughout the experiments include the gustatory stimuli [sucrose (0.1 M), NaCl (0.05 M), citric acid (0.01 M), and quinine (0.001 M)], which were presented at room temperature. All stimuli were purchased from Sigma-Aldrich (St. Louis, MO) and dissolved in deionized water to reach the final concentration. For the artificial saliva data, the composition of artificial saliva was based on Breza et al. (2010) and consisted of 0.015 M NaCl, 0.022 M KCl, 0.003 M $CaCl_2$, and 0.0006 $MgCl_2$ with pH 5.8 ± 0.2. Both gustatory stimuli and artificial saliva were freshly prepared each day.

**Electrophysiology data and statistical analysis**

Kilosort 2 (tetrode data) and Kilosort 3 (probe data) (Pachitariu et al. 2016) were used for automated spike sorting on a workstation with an NVIDIA GPU, CUDA, and MATLAB installed. Following spike sorting, the Phy software was used for manual curation. Finally, quality metrics and waveform properties were calculated using code based upon SpikeInterface (Buccino et al. 2020). Only units with an overall firing rate >0.3 Hz, signal-to-noise ratio >3.0, and an ISI violation rate <0.2 were used for the subsequent analyses. All following analyses were performed on custom Python and R scripts.

*Water-responsiveness.*

Water-responsiveness was assessed in all isolated neurons recorded ($n$ = 431 for data presented in Figs. 1–5; $n$ = 67 for data presented in Fig. 6; $n$ = 213 for data presented in Figs. 7–9). This analysis served only to estimate whether and how many GC neurons showed evoked activity that significantly differed from baseline for at least one of the temperatures tested, and not whether there was a significantly different response between the different thermal stimuli. Single-unit spike timestamps were aligned to the stimulus delivery, and peri-stimulus time histograms (PSTHs) were constructed (bin size = 250 ms). Significant changes from baseline were established using a Wilcoxon rank-sum comparison between baseline bin and evoked bin with correction for family-wise error (Bonferroni correction, $P < 0.01$). Latency onset was defined as the time in which the smoothed PSTH trace reached half of the max (for active responses where baseline firing rate < evoked firing rate) or the min (for suppressed responses where baseline firing rate > evoked firing rate) firing rate. For the PSTHs presented in Figs. 2C and 6C, population responses were obtained by averaging the auROC of each neuron in the observed population. The area under the receiver-operating characteristic (auROC) method normalizes the stimulus-evoked activity to the baseline on a 0 to 1 scale. A score of >0.5 is an active response and <0.5 is a suppressed response; 0.5 represents the median of equivalence of the baseline activity. For these normalized population PSTHs, a bin size of 100 ms was used.

*Temperature-selective neurons.*

To determine the degree of temperature specificity of GC water responses, we subjected each of the water-responsive neurons to a support vector machine (SVM) classifier, used and described in detail in a previous study (Neese et al. 2022). Briefly, the spike train dataset (0–1.5 s after water delivery) was transformed into a collection of vectors, each corresponding to one experimental trial. Each trial in the dataset was classified hierarchically according to neuron ID and temperature of water (labels: 14 °C, 25 °C, or 36 °C) for the trial. Thus, several vectors were associated with a single neuron, depending on how many trials were run with different temperatures. Then, for each single neuron, the classification analysis consisted of separating the ensemble of vectors into a training set consisting of 67% of the spike trains, and a testing set consisting of the remaining 33% of the spike trains. The training set was used to fit parameters for the SVM model (linear SVM kernel was used throughout our analysis); the SVM searched for hyperplanes that best separated the various classes (i.e. points corresponding to trials for different water temperatures) within the dataset. The trained model was then used to classify the testing dataset, resulting in a classification score measured as the percentage of correctly classified points. This procedure was repeated 20 times for each neuron, each time using a different partition of vectors into training and testing sets, and the classification scores were averaged over these trials to obtain an overall classification score for the neuron. To assess the significance of the overall classification score, we used a permutation test where the labels of the trials were shuffled without replacement. Spike trains were shuffled 100 times, and the pseudo-classification score index was calculated for each iteration of the shuffling. A neuron was deemed temperature selective if its overall classification score was >99%ile of the pseudo-classification scores ($P < 0.01$).

*Population decoding classifier.*

To understand how well the GC encoded information regarding oral temperature (Fig. 4), we used a population decoding approach. To this end, we first constructed a pseudo-population of GC neurons using temperature-selective neurons recorded

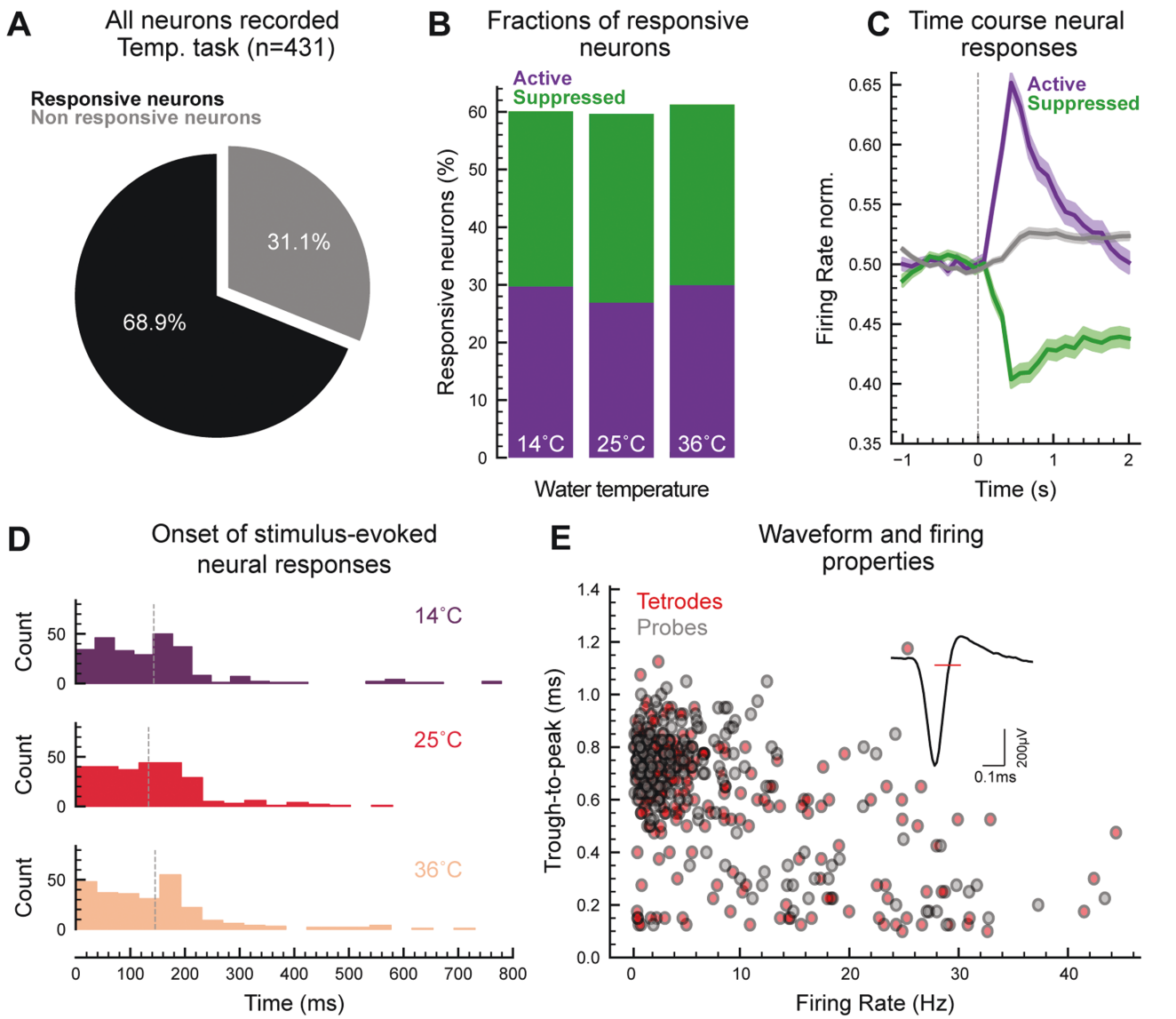


**Fig. 2.** Quantification of water responses in the mouse GC. (A) Pie chart showing the proportion of neurons modulated by at least one (14 °C, 25 °C, or 36 °C) oral thermal stimulus. (B) Bar plots displaying the proportion of responsive neurons showing either an active (*W.resp. active* in purple) or suppressed (*W.resp. supp.* in green) response to water at 14 °C, 25 °C, or 36 °C. (C) Population PSTHs of active (purple), suppressed (green), and nonresponsive (gray) GC neurons expressed as normalized firing rate (norm. FR). Shaded areas represent SE. (D) Distribution of onset response latencies. Vertical dashed lines represent mean values. (E) Scatter plot of the trough-to-peak duration and firing rate of all single neurons recorded. Red and gray dots represent neurons isolated from tetrode and probe recording sessions, respectively. The inset shows a representative example of a spike waveform with a red horizontal line highlighting the duration of the trough-to-peak interval.

across different sessions ($n$ = 179). We then generated a firing rate matrix (trials × time bin) where the spike timestamps of each neuron (2 s before and 2 s after stimulus) were realigned to water delivery, binned into 50-ms time bins. To assess the amount of temperature-related information, we used the SVM classifier described above. Spike activity data contained in our matrix were divided into a training set consisting of 67% of the spike trains and a testing set consisting of the remaining 33% of the spike trains. This process was repeated 20 times (each time using different training and testing splits) to compute the decoding accuracy, defined as the fraction of trials in which the classifier made correct temperature predictions using a 25-ms sliding window. To assess the significance of the population decoding over time, we used a permutation test where the labels of the trials were shuffled without replacement. Spike trains were shuffled 10 times, and the pseudo classification score over time was calculated for each iteration of the shuffling.

*Taste-selective neurons.*

In order to define a neuron as taste selective, 2 criteria must be satisfied: (i) activity significantly differs from baseline and (ii) there is a significantly different response among the 4 tastants. Significant changes from baseline were evaluated using Wilcoxon rank-sum comparison (Bouaichi and Vincis 2020) as already described in the *Water-responsiveness* sub-section of the Method section. Significant changes between tastes were determined using an SVM classifier (Neese et al. 2022) as already described in the *Temperature-selective neurons* sub-section of the Method section. To further investigate

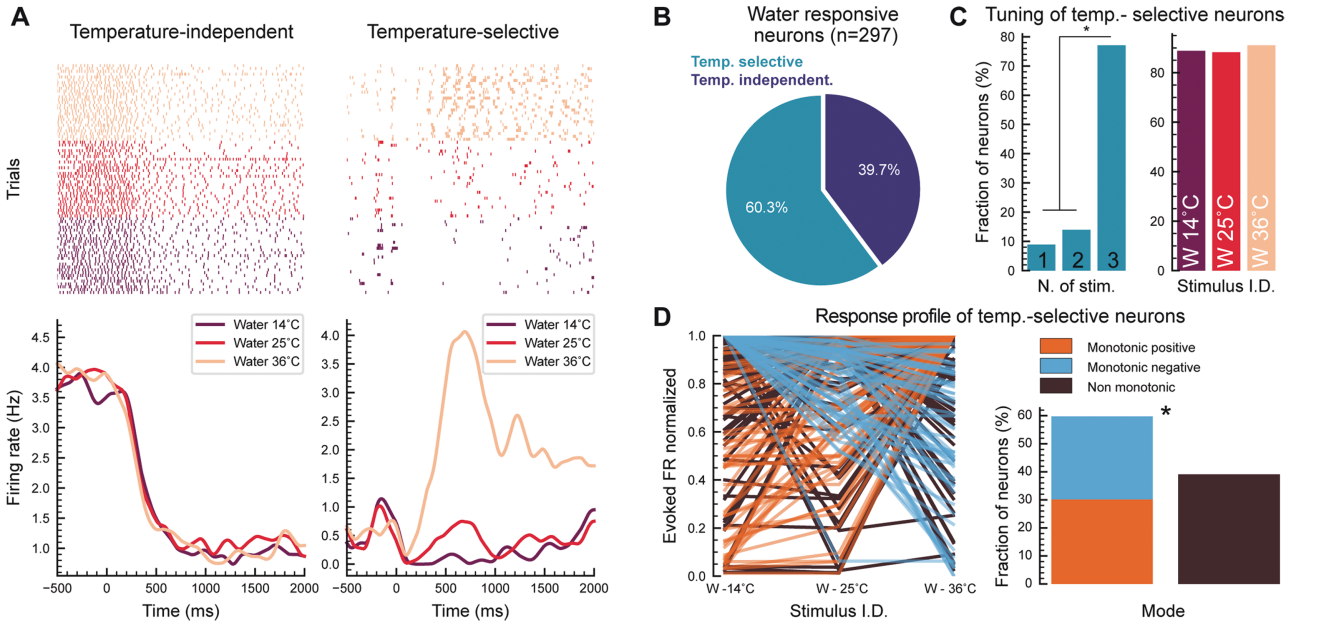


**Fig. 3.** Tuning of temperature-selective neurons in the gustatory cortex (GC). (A) Raster plots and PSTHs of 2 representative water-responsive GC neurons, showing temperature-independent (left) and -selective (right) responses. Trials pertaining to water at different temperatures are grouped together (in the raster plots) and color coded. (B) Pie chart displays the proportion of water-responsive neurons showing either temperature-selective (in light blue) or -independent (in dark blue) response to water. (C) *Left*—Fraction of temperature-selective neurons responding to 1, 2, or 3 thermal stimuli ($\chi^2$ test for given probabilities: $\chi^2 = 154.94$, df = 2, $P < 2.2e{-}16$; multiple proportion comparison—Marascuilo procedure, $P < 0.01$). *Right*—fraction of temperature-selective neurons responding to the 3 different temperatures of water ($\chi^2$ test for given probabilities: $\chi^2 = 0.0875$, df = 2, $P = 0.9572$). (D) *Left*—Plot of peak evoked firing rate (normalized) as a function of water temperature for all the temperature-selective neurons. *Right*—Quantification of the mode (monotonic vs. non-monotonic) of response for temperature-selective neurons in the GC ($\chi^2$ test for given probabilities: $\chi^2 = 7.7345$, df = 1, $P = 0.005418$).

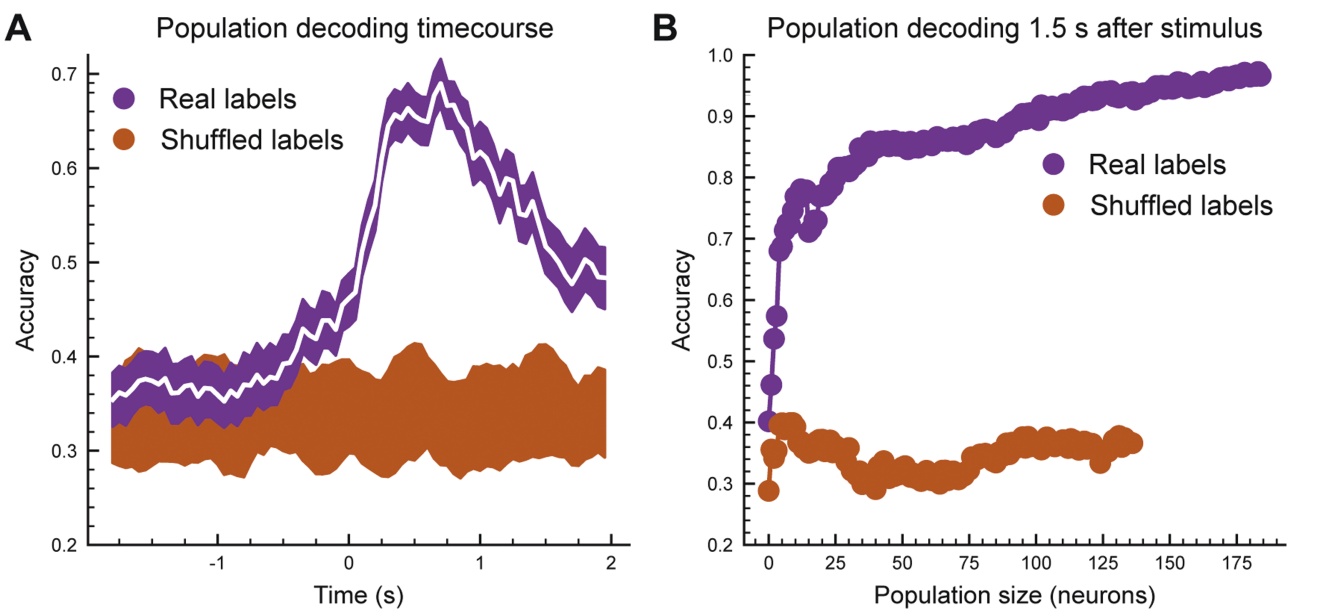


**Fig. 4.** Population decoding of oral thermal stimuli in the GC. (A) Time course of decoding performance (white line) considering the population of temperature-selective neurons. Purple-shaded area indicates the 1%ile to 99%ile range of the 20 times the decoder was ran, each time using different training and testing splits ($n = 20$). Brown-shaded areas indicate the 1%ile to 99%ile range of the decoding performance over time after shuffling (10 times) stimulus labels for all trials. (B) The mean accuracy of SVM linear decoders trained to discriminate the 3 different temperatures (using a temporal window of 1.5 s after stimulus) as the decoder gained access to progressively more neurons (purple dots). Brown dots indicate the decoding performance over time after shuffling (10 times) stimulus labels for all trials.

the taste response profile of taste-selective neurons, we used sharpness (SI) (Rainer et al. 1998; Yoshida and Katz 2011; Bouaichi and Vincis 2020) and palatability (PI) (Piette et al. 2012; Bouaichi and Vincis 2020) indices. SI was computed on the mean firing rate during the 1.5-s-wide interval after taste delivery and was defined as

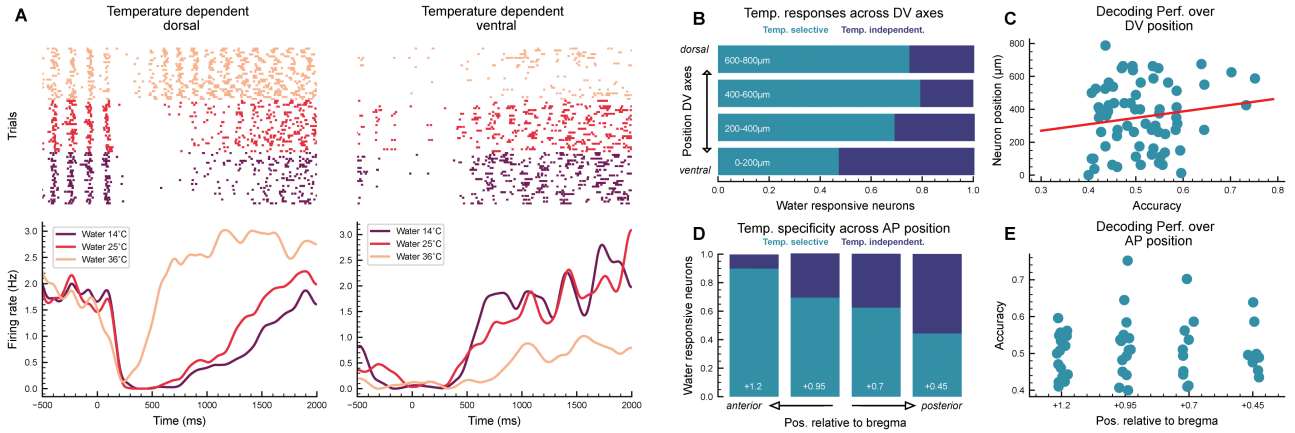


**Fig. 5.** Tuning of temperature-selective neurons across the GC axis. (A) Raster plots and PSTHs of 2 temperature-selective neurons, one recorded in the dorsal (*left)* and one in the ventral (*right)* GC. Water delivery trials at different temperatures are grouped together (in the raster plots) and color-coded (both in the raster plots and PSTHs). (B) Fraction of temperature-selective (light blue) and -independent (dark blue) neurons as a function of their dorso-ventral location (four 200-µm bins along the GC anterior–posterior axes; $\chi^2$ test for given probabilities: $\chi^2 = 8.506$, df = 3, $P = 0.03663$). (C) Scatter plot of the SVM accuracy for temperature-selective neurons against their dorso-ventral location (linear regression analysis: $R^2 = 0.02343$, $P = 0.2092$). (D) Fraction of temperature-selective and -independent neurons as a function of their antero-postero location ($\chi^2$ test for given probabilities: $\chi^2 = 9.2087$, df = 3, $P = 0.02664$). (E) Plot of the SVM accuracy for temperature-selective neurons against their antero-postero location.

$$\frac{n - \left(\sum \frac{\mathrm{Fr}_i}{\mathrm{FR}_b}\right)}{n-1}$$

where $\mathrm{Fr}_i$ is the mean firing rate for each taste ($i$ = 1–4), $\mathrm{FR}_b$ is the maximum firing rate among gustatory stimuli, and $n$ is the total number of stimuli ($n$ = 4). An SI of 1 indicated that a neuron responded to 1 stimulus (narrow tuning), and the value 0 indicated equal responses across stimuli (broad tuning). To evaluate whether taste-selective neurons encoded palatability-related information, we used the palatability index (PI). To avoid potential confounds introduced by differences in baseline and evoked firing rates across our pools of taste-selective neurons, we first normalized the PSTHs with the auROC procedure. To build the PI, we considered the time course of the difference of the PSTHs (100-ms bin) in response to gustatory stimuli of similar (sucrose–NaCl and citric acid–quinine) versus opposite (sucrose–quinine, sucrose–citric acid, quinine–NaCl, citric acid–NaCl) palatability (Bouaichi and Vincis, 2020). We computed the absolute value of the log-likelihood ratio of the normalized firing rate for each 100-ms bin for taste responses with similar ($|\mathrm{LR}|_{\mathrm{same}}$) and opposite ($|\mathrm{LR}|_{\mathrm{opposite}}$) hedonic values:

$$|\mathrm{LR}|_{\mathrm{same}} = 0.5 \times \left(\left|\ln \frac{\mathrm{sucrose}}{\mathrm{NaCl}}\right| + \left|\ln \frac{\mathrm{quinine}}{\mathrm{citric\ acid}}\right|\right)$$

$$|\mathrm{LR}|_{\mathrm{opposite}} = 0.25 \times \left(\left|\ln \frac{\mathrm{sucrose}}{\mathrm{quinine}}\right| + \left|\ln \frac{\mathrm{sucrose}}{\mathrm{citric\ acid}}\right| + \left|\ln \frac{\mathrm{NaCl}}{\mathrm{citric\ acid}}\right| + \left|\ln \frac{\mathrm{NaCl}}{\mathrm{quinine}}\right|\right)$$

We then defined the PI as $|\mathrm{LR}|_{\mathrm{opposite}} - |\mathrm{LR}|_{\mathrm{same}}$. Positive PI values suggested that a neuron responded similarly to tastants with similar palatability and differently to stimuli with opposite hedonic values. Negative PI values indicated the alternative scenario in which a neuron responded differently to stimuli of the same palatability and similarly to taste with different hedonic values. A neuron was deemed palatability related if its PI value after taste delivery (i) was positive and (ii) exceeded the mean + 6 × standard deviation of the PI values in the baseline for more than three 100-ms bins (Bouaichi and Vincis 2020).

### Histology

At the end of the experiment, mice were terminally anesthetized and perfused transcardially with 30 ml of PBS followed by 30 ml of 4% paraformaldehyde (PFA). The brains were extracted and post-fixed with PFA for 24 h, after which coronal brain slices (100-µm thick) containing the GC were sectioned with a vibratome (VT1000 S; Leica, Wetzlar, Germany). To visualize the tracks of the tetrode bundles and probes, brain slices were counterstained with Hoechst 33342 (1:5,000 dilution, H3570; Thermo Fisher, Waltham, MA) by standard techniques and mounted on glass slides. GC sections were viewed and imaged on a fluorescence microscope.

## Results

### Single neuron analysis of GC oral thermal responses

To investigate how single GC neurons encode oral thermal information in freely licking mice, we recorded ensembles of single units via movable bundles of tetrodes (Bouaichi and Vincis 2020; Vincis et al. 2020; Neese et al. 2022) or movable silicon probes (Cambridge Neurotech) mounted on a nanodrive shuttle (Cambridge Neurotech) implanted unilaterally in the GC (Fig. 1A). After habituation to head restraint, water-deprived mice were engaged in a behavioral task in which they had to lick 6 times to a dry spout to obtain a 3-µl drop of one oral fluid stimulus (Fig. 1B). On alternating days for up to 10 days, mice were trained to receive either 5 gustatory stimuli (0.1 M sucrose, 0.05 M NaCl, 0.01 M citric acid, 0.001 M quinine, and water) at room temperature (control session; Fig. 1A) or only water at 3 different temperatures (14 °C, 25 °C, or 36 °C; experimental session; Fig. 1A). During this training, tetrode bundles or silicon probes were slowly lowered to their final position (Fig. 1C) as described in the Methods section. At the end of the training, the recording session began. First, we recorded neural activity evoked by different taste qualities and water presented at room temperature (control session; Fig. 1D). After this recording session,

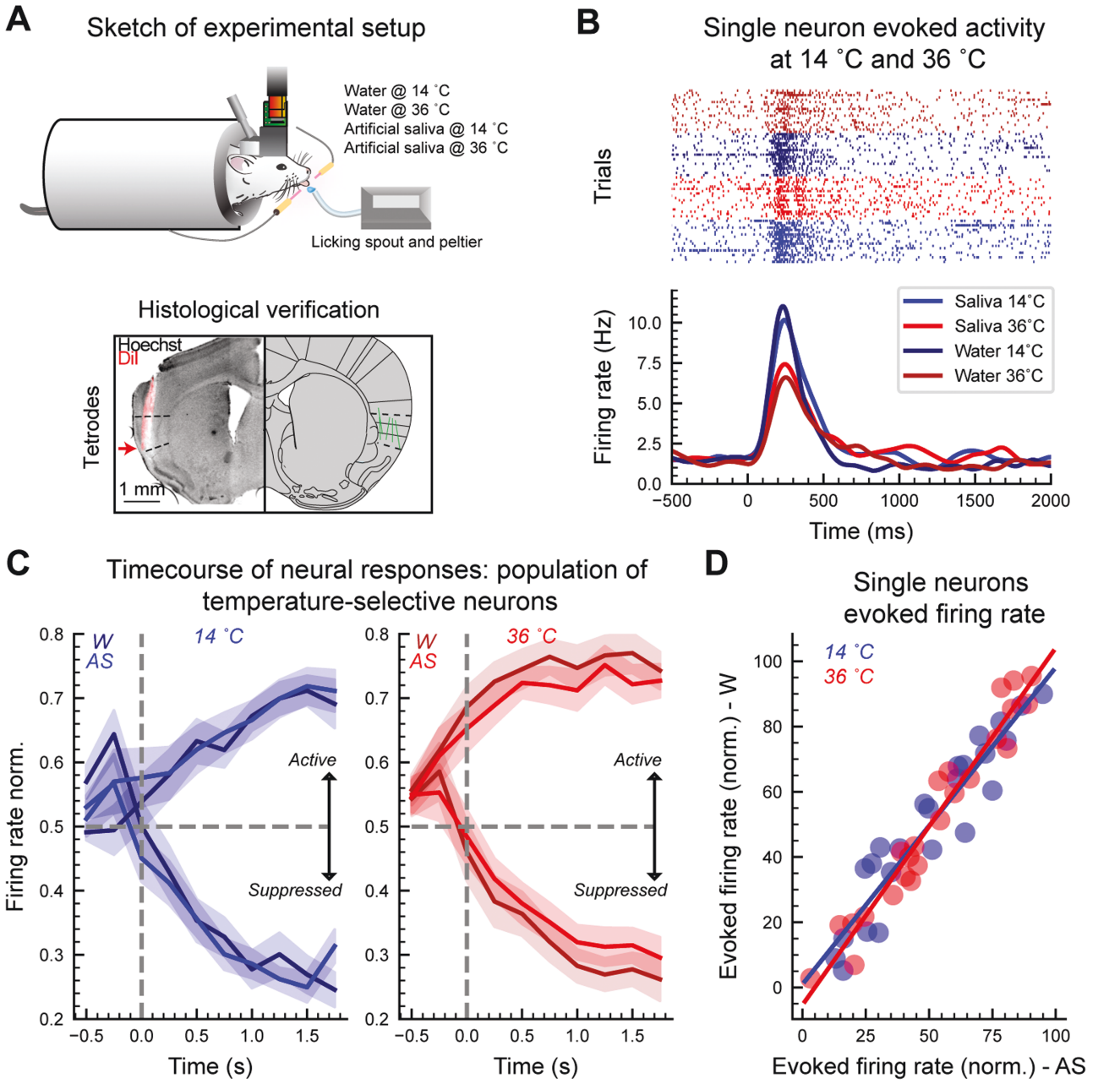


**Fig. 6.** Thermal responses evoked by deionized water and artificial saliva. (A) *Top*—Schematic showing the recording setup and a head-restrained mouse licking a spout to obtain deionized water or artificial saliva at 2 different temperatures (14 °C or 36 °C). *Bottom*—Example of one histological section showing a tetrode track (red) in the GC. Red arrow points to the tip of the tetrodes. On the far right, there is a schematic of the summary of the tetrode tracks from the 5 mice whose data are analyzed in Fig. 6. (B) Raster plot and PSTH of one temperature-selective neuron. Water and artificial saliva delivery trials at different temperatures are grouped together (in the raster plots) and color-coded (both in the raster plots and PSTHs). 36 °C trials are colored with red palette, with darker and lighter red for deionized water (W) and artificial saliva (AS), respectively. 14 °C trials are colored with blue palette, with darker and lighter red for deionized water (W) and artificial saliva (AS), respectively. (C) auROC-normalized population PSTHs showing active or suppressed responses after the presentation of deionized water or artificial saliva at 14 °C (*left*) and 36 °C (*right*). Vertical dashed lines indicate stimulus delivery (time = 0 s). Horizontal dashed lines indicate baseline. The shaded area represents the SEM. (D) Scatter plot showing the relationship between the firing rate evoked by artificial saliva (*x*-axis) and by deionized water (*y*-axis) at 14 °C (blue) and 36 °C (red). Each dot represents a temperature-selective neuron. The red and blue lines show the linear regression for 36 °C ($R^2$ = 0.9481, $P$ = 7.829e−16) and 14 °C ($R^2$ = 0.883, $P$ = 6.139e−12), respectively.

single neuron spiking activity was analyzed; if taste-selective neurons were detected, in the next recording sessions, we exclusively recorded activity evoked by water at the different temperatures (experimental session; Fig. 1E; 3 recording sessions for all mice except the ones implanted with the H5 probe; at the end of each experimental session, tetrodes and probes were lowered to record new ensembles of neurons [see Materials and Methods section for more details]). It is important to highlight we are not claiming to have tracked the same taste-selective neurons across multiple days and recording sessions. Rather, this approach was chosen exclusively to provide additional functional evidence to support

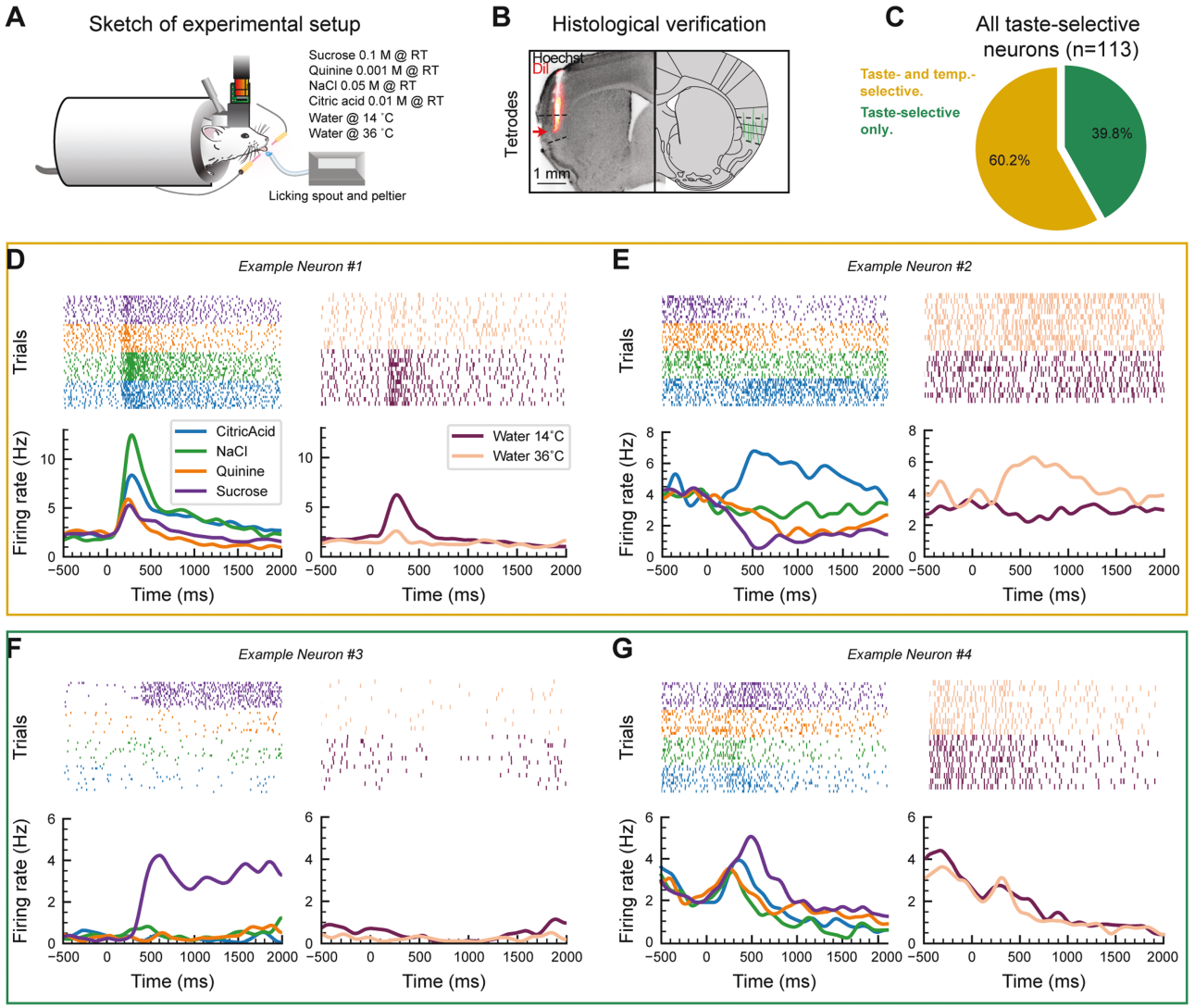


**Fig. 7.** Convergence of chemosensory and thermal oral stimuli in the GC. (A) Schematic showing the recording setup and a head-restrained mouse licking a spout to obtain deionized water (at 14 °C or 36 °C) or one of the 4 tastants. (B) *Left*—Example of one histological section showing a tetrode track (red) in the GC. Red arrow points to the tip of the tetrodes. *Right*—Schematic of the summary of the tetrode tracks from the 12 mice whose data are analyzed in Fig. 7. (C) Pie chart showing the proportion of taste-selective neurons ($n$ = 113) that are modulated exclusively by taste (taste-selective only) or by taste and thermal stimuli (taste- and temperature-selective). (D–E) Raster plots and PSTHs of 2 taste- and temperature-selective neurons (one neuron in panel D and one neuron panel E). Taste (*leftmost)* and water (*rightmost)* trials are separated for clarity. (F–G) Raster plots and PSTHs of 2 taste-selective only neurons (one neuron in panel F and one neuron panel G). Similar to panels D–E, taste (*leftmost)* and water (*rightmost)* trials are separated for clarity.

that recordings aimed at neuron responses to orally sourced thermal stimuli (experimental session; Fig. 1E) were indeed obtained from the GC. Overall, during recording sessions aimed at investigating thermal responses, a total of 431 single neurons were recorded from 16 mice with an average yield of 11.42 ± 6.49 neurons per experimental session.

To begin evaluating the neural dynamics evoked by oral thermal stimuli in active licking mice, we analyzed the spiking profile of single GC neurons. Figure 1E shows the raster plots and PSTHs of 2 representative GC neurons. Visual inspection of the graphs indicated that each of these neurons was modulated by different temperatures of water (Fig. 1E). As a first step, we wanted to understand how many GC neurons were modulated by the presence of a solution in the mouth. This analysis was performed by comparing the baseline and evoked neural activity from each of the 3 water temperatures and therefore serves only to estimate whether and how many GC neurons were responsive to oral thermal stimuli—not whether those responses differ as a function of the temperature of the stimulus. Wilcoxon rank-sum analysis revealed that a substantial number of the recorded GC neurons (68.9% [297/431]) responded to at least one of the 3 oral thermal stimuli and were classified as "water-responsive" (Fig. 2A). We observed a similar fraction of water-responsive neurons showing active and suppressed activity to each of the temperatures tested (Fig. 2B). Figure 2C shows the population averages (population PSTHs) of the active and suppressed responses. Analysis of the distribution of the latency of the responses indicated 2 main points. First, most of the water-responsive neurons showed a fast onset, with firing rate significantly changing from baseline within the first 200 ms after stimulus delivery (Fig. 2D; mean onset 0.29 ± 0.360 s).

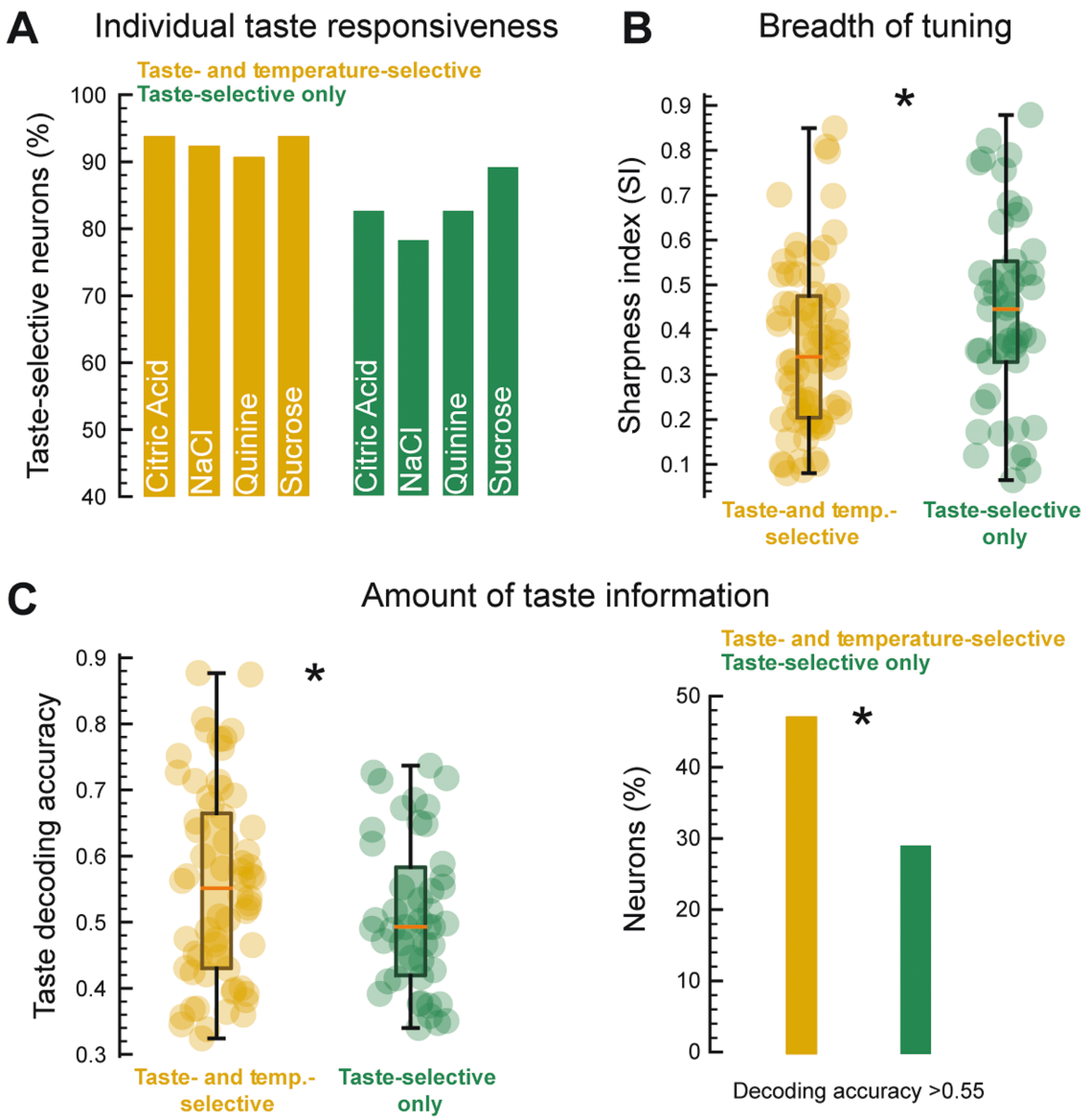


**Fig. 8.** Taste-selective properties of the 2 subsets of GC neurons. (A) Fraction of taste- and temperature-selective-only (gold) and taste-selective-only (green) neurons responding to the 4 different taste qualities. (B) Box plots showing the distribution of the breadth of tuning (expressed as sharpness index, SI) of the taste- and temperature-selective (gold) and taste-selective only (green) neurons. High SI values indicate narrowly responsive neurons, whereas low SI values imply that the neuron is modulated by multiple tastants. Each colored circle represents a single neuron. C: *left* - Box plots showing the distribution of the taste decoding accuracy of the taste- and temperature-selective (gold) and taste-selective-only (green) neurons. Each colored circle represents a single neuron. *Right*—Fraction of taste- and temperature-selective-only (gold) and taste-selective-only (green) neurons with a high (>[chance-level × 2]) decoding accuracy for taste information (2-sample test for equality of proportions: $\chi^2 = 3.011$, df = 1, $P = 0.04135$).

Second, the distribution of response latencies did not differ as a function of the temperature of the stimulus (Kruskal–Wallis $\chi^2 = 0.087628$, df = 2, $P = 0.9571$). Additionally, analysis of the distribution of 2 waveform properties (firing rate and trough-to-peak) revealed no differences in the population of neurons sampled via tetrodes and silicon probes (Fig. 2E; firing rate comparison, *t*-test: $t = 0.92692$, df = 380.99, $P = 0.3546$; trough-to-peak comparison, *t*-test: $t = -1.7226$, df = 427.94, $P = 0.08569$).

Next, we wanted to investigate the relationship between neural activity and oral thermosensation. To this end, we evaluated whether the evoked activity of water-responsive neurons differs as a function of the temperature of the water. A qualitative evaluation of the raster plots and PSTHs in Figs. 1 and 3 indicated that these responses can be classified as temperature independent (i.e. water responses appear to be similar at the 3 temperatures tested; see, for example, Fig. 3A—left) and as temperature-selective (i.e. evoked responses appear to differ as a function of the thermal stimulus; see, for example, Figs. 1E and 3A—right). To quantify the degree of temperature selectivity of GC neurons, we subjected each of the water-responsive neurons to an SVM classifier (Neese et al. 2022; see Materials and Methods for more details). The SVM uses a supervised machine learning algorithm that acts as a classifier whose performance was used as a surrogate for the ability of each individual neuron to encode thermal information in a 1.5-s post-stimulus temporal window. This analysis revealed that more than half of the GC water-responsive

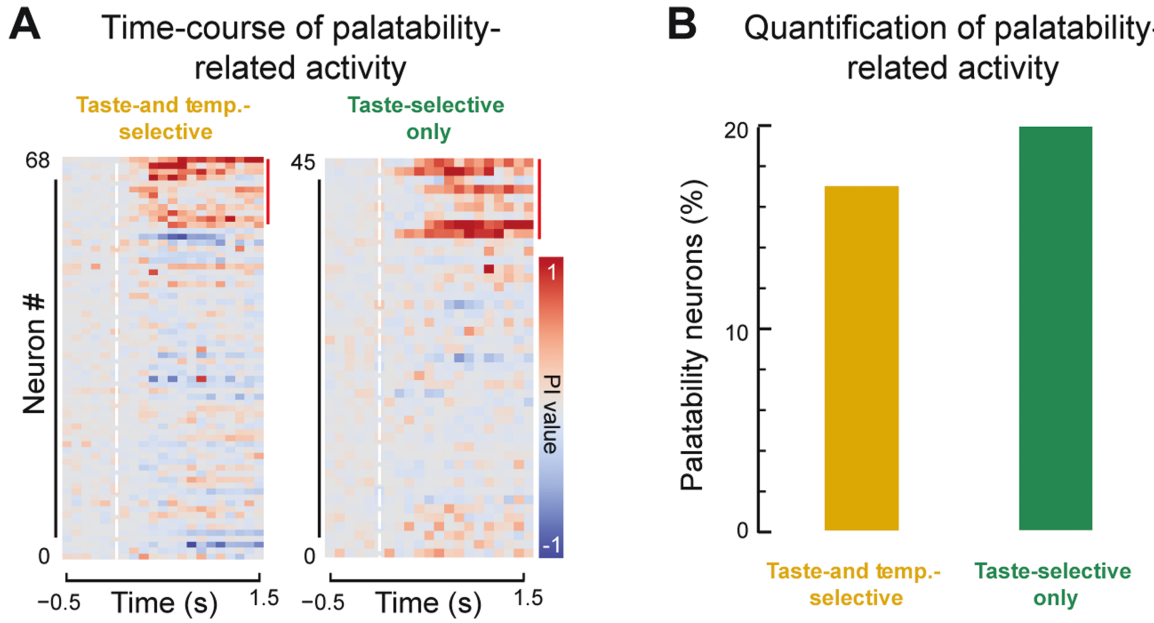


**Fig. 9.** Palatability coding in the 2 subsets of GC neurons. (A) Color-coded plots showing the time course of the PI index across 2 s around taste delivery at 0 s for all 64 taste- and temperature-selective neurons (*left*) and all 45 taste-selective-only neurons (*right*). Each row represents a single neuron; time 0 and white vertical dashed lines highlight taste delivery. Thick red vertical lines on the top right corner of each plot indicate the neurons deemed palatability-encoding. (B) Bar graph showing the fraction of the palatability-encoding neurons of the taste- and temperature-selective (gold) and taste-selective-only (green) neurons.

neurons (60.3%, 179/297) were temperature-selective (Fig. 3B), whereas the remaining (39.7%, 118/297) likely encoded for thermal-independent features. We then wanted to understand if the temperature-selective GC neurons were preferentially modulated by only a specific temperature or if they were capable of encoding information pertaining to multiple thermal stimuli. This analysis serves only to estimate how many temperature-selective neurons were modulated by more than one thermal stimulus, independent of the degree of the temperature. The distribution plot shown in the left panel of Fig. 3C indicates that the majority of temperature-selective neurons were capable of responding to all 3 of the temperatures tested (Fig. 3C—*left*; $\chi^2$ test for given probabilities: $\chi^2 = 154.94$, df = 2, $P < 2.2e{-}16$; Multiple proportion comparison—Marascuilo procedure, $P < 0.01$).

Next, we wanted to evaluate if GC temperature-selective neurons were tuned to both cooling and warming oral stimuli or if they preferentially responded to either one. When we considered the absolute values of the water stimulus (14 °C, 25 °C, or 36 °C), we observed that temperature-selective neurons were broadly responsive to all thermal stimuli, independent of the degree (°C) value (Fig. 3C—*right;* Chi-squared test for given probabilities: $\chi^2 = 0.0875$, df = 2, $P = 0.9572$). If instead we consider deviation from resting oral temperature (32 °C (Leijon et al. 2019); $\Delta T$), more GC neurons appear to be tuned to cooling (<32 °C) than to warming (>32 °C) stimuli. However, this latter observation might be biased due to the limited and uneven set of stimuli used (14 °C and 25 °C are both "cooling" and 36 °C is "warming"; see the Discussion section for more on this point). To further investigate how GC temperature-selective neurons were tuned to absolute changes in orally sourced temperature of fluid solution, we performed an additional analysis: we evaluated if the neuron's firing either positively or negatively correlated with increase of temperature (monotonic) or not (non-monotonic). Our analysis revealed that most of the temperature-selective neurons changed their firing rate in a monotonic fashion (Fig. 3D; Chi-squared test for given probabilities: $\chi^2 = 7.7345$, df = 1, $P = 0.005418$). Overall, these analyses revealed that most of the GC neurons that responded to the delivery of water were temperature-selective and capable of encoding different absolute temperature values in a mostly monotonic manner.

## Population coding for oral temperature in GC

To further characterize cortical thermosensory processing, we performed a population decoding analysis. The decoder was instantiated using the same SVM classifier described above for single neurons; the difference in this case is that the classifier was trained using single trial responses of pseudopopulations of temperature-selective GC neurons (neurons pooled from different experimental sessions and animals) and tested using a held-out method (training set consisting of 67% of the spike trains and a testing set consisting of the remaining 33% of the spike trains). This process was repeated 20 times (each time using different training and testing splits) to compute the decoding accuracy, defined as the fraction of trials in which the classifier made correct temperature predictions. We began by analyzing how well the population activity of temperature-selective neurons ($n = 179$) represented the 3 thermal stimuli over a 2-s long post-stimulus temporal window (Fig. 4A). Figure 4A shows the decoding performance of the pseudopopulation using a sliding window of 25 ms (white trace [average accuracy over the 20 training and testing splits] over the purple shading [1%ile (lower bound) and 99%ile (upper bound) of the 20 training and testing splits]). As a control, the same analysis was performed another 10 times after shuffling the thermal stimuli labels; the brown shaded area in Fig. 4A shows the 1%ile (lower bound) and 99%ile (upper bound) of the distribution of the control decoding values over time. The decoding time-course showed

an early onset (classification above control) and reached its peak within 1 s after stimulus delivery. Additionally, although the overall classification value started decreasing after 500 ms, decoding performances remained above control until the end of the temporal window analyzed (Fig. 4A). Figure 4B shows how classification during a 1.5-s post-stimulus temporal window changed as the decoder gained access to progressively more neurons. While the classifiers that trained with a small number of neurons were less accurate at identifying oral thermal information, increasing the number of neurons in the pseudopopulation drastically increased the decoding performance, reaching up to 85% accuracy with less than 40 neurons (Fig. 4B, purple dots). As expected, the decoding performance obtained with the control data did not improve and stayed around chance level even when the decoder gained access to progressively more neurons (Fig. 4B, brown dots). Taken together, these results indicate that both individual and ensembles of temperature-selective GC neurons rapidly and reliably encoded oral thermosensory signals over time, with classification accuracy for stimulus identity remaining above chance and control level for up to 2 s after stimulus delivery.

## Spatial organization of oral thermal responses

Next, we sought to determine whether oral responses were topographically organized. A previous study in anesthetized rats suggested that thermal responses in the GC are mostly clustered in the dorsal (granular) region (Kosar et al. 1986). However, it is still unknown whether oral thermal responses in behaving mice are also organized with a seemingly topographical gradient along the dorso-ventral axes of the GC.

To address this question, we took advantage of the recording sessions performed with chronic probes that allowed us to triangulate the location of the recorded neurons along the dorso-ventral axes spanning up to 800 µm (see Materials and Methods section for more details). Visual inspection of spiking activity shown in Fig. 5A indicated the presence of temperature-selective neurons in the dorsal and ventral region of the GC. We divided the dorso-ventral axes of the portion of the GC captured by our recording into four 200-µm spatial bins (Fig. 5B,C). Our post hoc evaluation of the implant tracks confirmed that the most ventral position was well within the agranular region of the GC (Fig. 1C). Overall, our probe recordings spanned 800 µm, which covered a large portion of the dorso-ventral plane of the mouse GC (Wang et al. 2020). Analysis of the temperature-selective neurons along the GC dorso-ventral axes reflected a coarse, and relatively weak, topographical organization with much fewer temperature-selective neurons in the most ventral part of GC (0 to 200 µm) compared with the other 3 spatial bins analyzed (Fig. 5B; 4-sample test for equality of proportions: $\chi^2 = 8.506$, df = 3, $P = 0.03663$). To further investigate between temperature-selective neurons and their location along the GC dorso-ventral axes, we plotted the single neuron SVM decoding accuracy against the neuron position (Fig. 5C). We reasoned that a topographical clustering might also appear when considering the amount of thermal-related information (expressed as decoding accuracy) of the temperature-selective neurons (e.g. neurons with high accuracy could cluster more dorsally). Contrary to our prediction, visual inspection of Fig. 5C and linear regression analysis ($R^2 = 0.02343$, $P = 0.2092$) revealed that was not the case. We then focused our attention on the organization of oral thermal responses along the rostro-caudal axes. Recent studies have started to uncover the role of the mouse posterior insular cortex in skin warming and cooling (Beukema et al. 2018; Vestergaard et al. 2023). To determine if oral thermal responses in the GC are organized in an antero-postero gradient, we analyzed the temperature-selective neurons recorded with the P1 probe (Fig. 1C) that allowed us to examine responsiveness along 1 mm of the GC antero-postero axes. Analysis of the distribution of temperature-selective neurons (Fig. 5D) revealed an antero-postero gradient with more temperature-selective neurons in the anterior GC (Fig. 5D; 4-sample test for equality of proportions: $\chi^2 = 9.2087$, df = 3, $P = 0.02664$). However, similar to what we observed for the dorso-ventral axes, the capability of GC neurons to decode thermal information did not depend on their position along the antero-postero axes (Fig. 5E; one-way ANOVA: $F(3,48) = 0.239$, $P = 0.869$).

In summary, these results suggest that the number of temperature-selective responses are, for the most part, sensitive to anatomic location within the mouse GC. The ratio of temperature-selective and temperature-independent neurons indicate that there is a coarse organization along the dorso-ventral and antero-postero axes. However, taste-sensitive neurons appear to encode thermal information (as revealed by the SVM classifier) equally well no matter location within the mouse GC.

## Comparison of oral thermal activity evoked by deionized water and artificial saliva

Water-specific responses have been reported in many brain regions of the gustatory neuraxis (Nakamura and Norgren 1991; Gutierrez et al. 2010; Rosen et al. 2010; Zocchi et al. 2017; Bouaichi and Vincis 2020; Neese et al. 2022); in addition, previous studies have argued (Accolla et al. 2007) and provided evidence (Zocchi et al. 2017) in favor of water as an independent taste quality. Therefore, we sought to understand if the temperature-selective activity observed so far in the GC neurons was mostly driven by thermal information in absence of an overt taste stimulus (as opposed to "taste"—temperature integration). To this end, we designed an experiment that allowed us to compare thermal responses with water to those with artificial saliva—another oral stimulus often used as a neutral control instead of deionized water in taste research (Breza et al. 2010; Baumer-Harrison et al. 2020; Travers et al. 2022). We recorded neural activity from GC neurons ($n = 67$) of a second group of mice ($n = 5$) trained to receive deionized water or artificial saliva at 14 °C or 36 °C (Fig. 6A). Figure 6B shows the raster plots and PSTHs of one temperature-selective GC neuron. A qualitative analysis of the single neuron's thermal responses indicated that neural activity evoked by deionized water and artificial saliva was very similar (Fig. 6B). Next, we wanted to evaluate the similarity between the activity evoked by water and artificial saliva at the 2 temperatures in all temperature-selective neurons. Figure 6C shows the auROC-normalized population (all temperature-selective neurons) averages of the time course of the responses to 14 °C and 36 °C, further highlighting the similarity of the neural activity evoked by deionized water and artificial saliva (Fig. 6C). To perform a quantitative evaluation of the similarity of the neural activity, we used a linear regression to test if the evoked firing rate in the 1.5-s temporal window—with water as stimulus—significantly predicted the evoked firing rate of artificial saliva (Fig. 6D). For both 14 °C and 36 °C, the overall

regression was statistically significant (14 °C: $R^2$ = 0.883, $P$ = 6.139e–12; 36 °C: $R^2$ = 0.9481, $P$ = 7.829e–16), indicating that temperature-selective neurons in the GC showed a high degree of similarity in their responses to water and artificial saliva and appear to encode oral thermal information in the absence of overt chemosensory taste stimuli.

## Evaluating the convergence of thermal and chemosensory information on GC neurons

While our results thus far have described how orally sourced thermal inputs are processed in the GC, this cortical region is typically studied for its role in processing chemosensory taste information (Katz et al. 2001; Stapleton et al. 2006; Jezzini et al. 2013; Bouaichi and Vincis 2020; Neese et al. 2022). In addition, recent electrophysiological studies suggest that GC neurons are capable of integrating multimodal intraoral signals (Vincis and Fontanini 2016a; Maier 2017; Samuelsen and Vincis 2021). Therefore, we next explored whether—and to what extent—thermal and chemosensory information converge on the same GC neurons. To accomplish this, we recorded neural activity from GC neurons of a third group of mice ($n$ = 12; 4 of these mice were also used for data presented in Fig. 6) trained to receive—in the same experimental session—a palette of 6 oral stimuli: 4 chemosensory taste stimuli presented at room temperature (sucrose, 0.1 M; NaCl, 0.05 M; citric acid, 0.01 M; quinine, 0.001 M) and 2 thermal stimuli (deionized water at 14 °C and 36 °C) (Fig. 7A, B). The concentration and temperature of the taste stimuli were chosen to provide compatibility to prior awake-behaving taste electrophysiology studies in mice (Levitan et al. 2019; Bouaichi and Vincis 2020; Dikecligil et al. 2020; Neese et al. 2022). Out of the 213 single neurons recorded, 113 were taste-selective. Taste-selective neurons were required to satisfy 2 criteria: they must have exhibited a significant firing rate change from baseline (defined by Wilcoxon rank-sum; Bouaichi and Vincis 2020), and they must have shown significantly different responses to the 4 tastants (defined by the SVM analysis; Neese et al. 2022). Furthermore, more than half (60.2%, 68/113) of the taste-selective neurons were also temperature-selective (Fig. 7C); these neurons will hereafter be referred to as taste- and temperature-selective neurons. Figure 7D and E shows the raster plots and PSTHs of 2 representative taste- and temperature-selective neurons. Visual inspection of the graphs indicated that each of these neurons was modulated by different taste stimuli and by the 2 different temperatures of water. On the contrary, 39.8% (45/113) of taste-selective neurons were not modulated by the thermal inputs (Fig. 7C) and were therefore deemed taste-selective only neurons. Representative examples of this category of GC neurons are shown in Fig. 7F and G. These qualitative results started to paint a picture wherein the majority of GC neurons that encoded taste information were also capable of integrating oral thermal stimuli. To further explore this idea, we performed a series of analyses aimed at understanding whether the GC neurons that responded to both taste and thermal information represented a unique population of taste-selective cells. First, we aimed to evaluate if either of the 2 sets of GC neurons (taste- and temperature-selective neurons and taste-selective only neurons) were differently tuned to encode information pertaining to individual taste qualities. Figure 8A shows that both groups of neurons responded to gustatory stimuli independent of their chemical identity, and the total fraction of taste-selective-only neurons modulated by each taste stimulus was lower than the taste- and temperature-selective neurons. We reasoned that this latter point could be the result of taste-selective-only neurons being more narrowly tuned. Thus, to further investigate differences in the tuning profiles of taste-selective neurons, we computed the response sharpness index (SI), a standard technique used to evaluate the breadth of tuning of single neurons (Yoshida and Katz 2011; Wilson and Lemon 2013) (Fig. 8B), for each taste-selective neuron. High SI values are evidence of narrowly tuned neurons (i.e. GC neurons that encode 1 taste stimulus), whereas low SI values indicate broadly tuned neurons (i.e. GC neurons that encode multiple taste stimuli).

Figure 8B shows the distribution of SI values for the 2 taste-selective groups. In agreement with our hypothesis, we observed that the taste- and temperature-selective neurons are more broadly tuned (2-sample $t$-test: $t$ = –2.0104, df = 111, $P$ = 0.02341). These findings indicate that, with respect to their taste tuning profile, the taste- and temperature-selective neurons appear to be more broadly tuned, capable of being activated by more gustatory stimuli.

The above-analysis examines only responsiveness, providing no direct information regarding whether the 2 groups of taste-selective neurons differ in how well they can encode taste information. We therefore performed a comparison of the distribution of the taste decoding accuracy for each of the taste-selective neurons (Fig. 8C—*left)*. The decoding accuracy (computed with SVM, see Methods for more details) is a surrogate for the ability of each individual neuron to encode gustatory information in a 1.5-s post-stimulus temporal window. Visual examination of the data suggests that the spiking activity evoked by the gustatory stimuli in the taste- and temperature-selective neurons contains a greater amount of taste information. A non-paired $t$ test confirmed the latter observation (2-sample $t$-test: $t$ = 1.7664, df = 111, $P$ = 0.04004). This result is confirmed when comparing the fraction of taste-selective neurons with decoding accuracy of >0.55 (more than 2× chance level) (Fig. 8C—*right*; 2-sample test for equality of proportions: $\chi^2$ = 3.011, df = 1, $P$ = 0.04135). Taken together, these observations indicated that GC neurons that were modulated by both chemosensory and thermal oral inputs were more effective in coding taste information than the GC neurons that responded only to gustatory inputs. We next sought to evaluate if the 2 populations of taste-selective neurons also differed in their capability of encoding information about taste palatability. Previous studies have indicated that GC neurons are capable of representing the palatability of intraoral taste stimuli (Katz et al. 2001; Bouaichi and Vincis 2020) and that cooler temperatures of fluid solutions are preferred by water-deprived rats (Torregrossa et al. 2012). On the basis of these studies, we hypothesized that the time course of taste- and temperature-selective neuron responses would contain more palatability-related activity. We further reasoned that, if the latter hypothesis was confirmed by the data, it would shed some light in the direction of GC thermal responses representing mostly the reward—and less the sensory properties—of the oral thermal stimuli. To quantify the numbers of GC neurons showing palatability-related activity, we computed the time course of the PI (Jezzini et al. 2013; Liu and Fontanini 2015; Bouaichi and Vincis 2020). This analysis was based on extracting the taste response similarity for each taste- and temperature-selective ($n$ = 68) and taste-selective

only ($n$ = 45) neuron for 100-ms-long time bins; positive PI implied palatability-related information while negative PI indicated inverse palatability coding. After computing the time course of the PI index, a neuron was deemed as encoding palatability if (i) it had a mean stimulus-evoked positive PI and (ii) it had a PI significantly above baseline for at least three 100-ms-long time bins. Figure 9A shows the time course of the PI index for the 2 groups of taste-selective neuron; visual inspection of the plots indicated that the taste-evoked activity in a subset of neurons in both groups contained palatability information. However, contrary to our prediction, a 2-sample $t$ test comparing the fractions of palatability-encoding neurons revealed no differences between the taste- and temperature-selective- and taste-selective-only neurons (Fig. 9B; 2-sample test for equality of proportions: $\chi^2$ = 0.0045921, df = 1, $P$ = 0.946).

While these analyses aimed to evaluate the level of convergence of taste and thermal information on individual GC neurons by focusing on the 113 taste-selective neurons shown in Fig. 7C, it was unclear whether the remaining 100 cells that were not taste-selective might have responded to temperature. Additional analysis revealed that 26% (26/100) of GC neurons that were not modulated by a taste stimulus were temperature-selective, indicating the presence of temperature-sensitive cells embedded among taste-selective cells.

Taken together, these observations indicate that taste- and temperature-selective neurons may represent—with respect to their taste responsive profile—a distinct set of broadly tuned neurons that can encode taste quality with high accuracy and may also participate in integrating taste quality with stimulus temperature.

## Discussion

This study evaluated the neural representations of oral thermal stimuli in the GC of behaving mice. We observed that GC neurons, as single units and as ensembles, were capable of reliably responding to and discriminating a wide range of innocuous oral temperatures of deionized water in a mostly monotonic manner. Oral responses appear to be distributed across the GC with the presence of an antero-postero gradient and a coarse dorso-ventral organization. Analyses of the similarity between the responses evoked by deionized water and artificial saliva revealed that, for the most part, temperature-related activity is driven by the thermal feature of the stimulus and not by the integration of the "taste of water" (Zocchi et al. 2017) and temperature. Finally, our data indicate that thermal stimuli can recruit GC neurons that also respond to taste. Comparison of the response profiles of the GC neurons representing these 2 forms of oral stimuli and that of those being modulated exclusively by tastants revealed different taste quality coding and tuning properties, with taste- and temperature-selective neurons appearing more broadly tuned and capable of encoding more information than their taste-selective only counterparts; neither taste-selective group, however, seemed to encode more information about palatability than the other. Altogether, our findings demonstrate that the GC of behaving mice is involved in processing oral information that could be relevant to ingestive behaviors (Torregrossa et al. 2012; Lemon 2021). This work represents the first effort to reveal details of the cortical code for the mammalian oral thermosensory system in behaving mice and paves the way for future investigations on the cortical circuits and operational principles underlying thermogustation.

### Oral thermosensory coding in GC

Our results indicate that the GC integrates thermal information in the absence of an overt taste stimulus (Figs. 1–5). More than half of the GC neurons that were modulated by the contact of a 3-µl droplet of deionized water within the oral cavity were temperature-selective (Fig. 3B). It is important to note that some studies argue that water may be considered as an independent taste quality (Accolla et al. 2007; Zocchi et al. 2017) and others have reported water-evoked responses along the gustatory neuraxis (Rosen et al. 2010; Bouaichi and Vincis 2020). With this in mind, we compared the responses of neurons in the GC to different temperatures of deionized water and artificial saliva and found the evoked neural responses to be very similar. Indeed, a linear regression using deionized water at 14 °C and 36 °C as a stimulus significantly predicted the evoked firing rate for the same temperature of artificial saliva (Fig. 6D). We can, therefore, more confidently argue that the temperature-selective neurons recorded in the GC appear to encode mostly oral thermosensory information. The question that then arises is, what are the functions of the thermal oral signals that GC neurons may be representing? The first is stimulus identification, which involves sensory-discriminative processes aimed at qualitatively distinguishing between fluid temperature. When considering the temperatures used in our study in absolute terms, we observed GC responses to all 3 temperatures with often the same neurons capable of representing more than one stimulus (Fig. 3C). When considering the degree of thermal change (i.e. $\Delta T$) achieved during stimulation from resting oral temperature [32 °C, (Leijon et al. 2019)], more GC neurons appear to be tuned to cooling (<32 °C) than to warming (>32 °C) stimuli. One challenge in the interpretation of this latter point is that we have not tested if our results generalize across a wider range of temperatures. For example, recent *in vivo* studies have shown that a subset of neurons in the trigeminal ganglion and the parabrachial nucleus of the pons (PBN) also respond to noxious cold (<14 °C) and hot (>40 °C) intraoral stimuli (Lemon et al. 2016; Yarmolinsky et al. 2016; Leijon et al. 2019; Li and Lemon 2019; Lemon 2021). The experimental design of the current work did not allow this level of analysis. We purposefully chose to omit noxious thermal stimuli to avoid distress for the mice and allow them to be engaged in the task and actively lick for a substantial number of trials. Another feature the GC may be encoding is the hedonic property of oral temperature. The thermal responses observed in our study could mostly reflect the hedonic—rather than the sensory quality—feature of the stimulus. Along this line, it is well established that GC neurons are capable of representing palatability of intraoral taste stimuli (Katz et al. 2001) and that cooler temperatures of fluid solutions are preferred by water-deprived rats (Torregrossa et al. 2012). As a result, one can expect a degree of convergence of taste and thermal stimuli onto palatability-related GC neurons. However, such an interpretation does not apply to our data. Indeed, GC neurons encoding both taste and temperature do not show a higher PI as compared to the ones encoding only gustatory stimuli (Fig. 9).

Delving further into these taste-selective neurons, we show that oral thermal stimuli can modulate GC neurons that

encode taste information (Figs. 7–9). Indeed, our results indicate that oral chemosensory and thermal inputs do not necessarily recruit distinct sets of GC neurons, but—for the most part—rather converge on the same cells. While this observation is in contrast with earlier reports (Kosar et al. 1986), it dovetails nicely with more recent studies highlighting the multimodal nature of many individual neurons in the GC (Vincis and Fontanini 2016a; Samuelsen and Fontanini 2017; Samuelsen and Vincis 2021). Analysis of the taste-quality response profiles between GC neurons modulated by both oral stimuli (taste- and temperature-selective) and the ones encoding only taste information (taste-selective only) revealed some differences. While in both groups the majority of neurons were modulated by more than one taste quality (Fig. 8A), they differed in their breadth of tuning. Specifically, the GC neurons that were exclusively modulated by tastants (but not temperature; taste-selective only neurons) appeared to be more narrowly tuned (Fig. 8B). This observation agrees with a previous report showing that GC neurons modulated by retronasally delivered odor and taste are more broadly tuned to gustatory stimuli than the unimodal (i.e. modulated by taste only) neurons (Samuelsen and Fontanini 2017). In addition, further analysis revealed that taste- and temperature-selective neurons encode taste quality—but not palatability-related—information with higher accuracy (Fig. 8 and 9). While we cannot yet provide definitive proof of the functional dissociation of the 2 groups of taste-selective neurons, we can speculate about their role in taste processing. GC neurons that encode both oral stimuli appear to be more broadly tuned within (taste quality) and across modality (taste and thermal inputs), and they may play a role in (i) the temperature–taste integration by linking thermal inputs to taste qualities, as well as in the "flavor network" (Small 2012; Samuelsen and Fontanini 2017; Samuelsen and Vincis 2021), and (ii) representing the neural substrate upon which associative flavor-related learning can operate (Vincis and Fontanini 2016a). Taste-only neurons (as defined by the analyses presented in this article) may primarily encode 1 or 2 taste qualities in a way that is independent of their temperature or association with any other intraoral flavor-related sensory cue (Samuelsen and Fontanini 2017). However, future experiments will test the equally likely event that thermal variation of the gustatory stimuli (not tested in this manuscript; see "A taste of things to come" section of the discussion) may modulate their taste response.

### Spatial organization of orally sourced thermal responses

Pioneering works in anesthetized rats have indicated that changes in intraoral temperature modulate the activity of a limited number of GC neurons (Yamamoto et al. 1981; Kosar et al. 1986). Interestingly, Kosar et al. provided some experimental evidence in support of a clear topographical organization of responses to intraoral stimuli. Their findings showed that, in the GC of anesthetized rats, thermal responses were not organized in a rostro-caudal fashion but rather appeared to be exclusively clustered dorsally (corresponding to the granular portion of the GC); taste responses, however, were clustered in the ventral agranular region (Kosar et al. 1986). To evaluate if oral thermal responses are topographically organized in the mouse GC, we performed a subset of electrophysiological recordings using linear and multi-shank silicon probes. With this approach, we relied on the high density of electrode contacts that allowed us to detect each spike at multiple sites, providing an opportunity to "triangulate" the location of each spike and to infer the relative 3D position of each single neuron. Our data revealed that temperature-selective activity along the dorso-ventral axis of the GC is mostly distributed with the exception of the most ventral portion of the GC, where there were more neurons responding to water in a temperature-independent manner (Fig. 5B). In addition, single neuron decoding revealed that the amount of temperature-selective information did not depend on the dorso-ventral position of the neuron (Fig. 5C). These findings appear to be partially in conflict with the one from Kosar et al. for at least 2 reasons. First, as already mentioned above, the distribution of temperature-selective neurons across the dorso-ventral axis in our study appears, for the most part, uniform. Second, our data indicate there is a high degree of convergence of taste and thermal responses in the same GC neuron (Fig. 8). This latter result—while in conflict with Kosar et al. where taste responses appeared to be exclusively clustered in the most ventral part of the rat's GC—agrees with other studies in mice showing that spatial location plays no role in the distribution of taste responses (Levitan et al. 2019; Chen et al. 2021) [but see Chen et al. (2011)]. It is important to highlight that the apparent lack of dorso-ventral topographical organization of thermosensory responses shown in our data does not necessarily exclude the possibility of the existence of subtle differences among GC subregions (granular, dysgranular, and agranular) or between the GC of different rodent models. Future experiments should endeavor to further probe these possibilities.

A recent study has shown that the posterior insular cortex—a cortical region rostral to the most posterior portion of the GC analyzed in this study—contains the primary cortical representation of skin temperature (Vestergaard et al. 2023). Interestingly, within the posterior insular cortex, body temperature appears to be topographically organized with thermal information from the paws being represented more posterior than the one originating from the face (Vestergaard et al. 2023). In our study, we investigated neural responses to oral thermal stimuli, focusing our attention on the GC that, as already mentioned above, is located rostral to the posterior insula region. While, in our study, temperature-selective neurons encoded oral fluid with high accuracy irrespective of their antero-postero axis (Fig. 5E), there was a responsiveness gradient with more neurons being modulated by at least one temperature in the anterior part of the GC (Fig. 5D). It is thus tempting to speculate about the existence of a topographical organization of temperature in the broad insular cortex with a potential postero-antero gradient reflecting an extraoral to oral transition of thermal information.

### Origin of thermosensory responses in the GC

It is likely that one of the neural circuits allowing thermal information to reach the GC is in part the ascending gustatory pathway. Changes in intraoral temperature can stimulate somatosensory neurons of the trigeminal system, which are responsible for thermosensation of all oral surfaces (Lemon 2021). In vivo experiments in mice have revealed that neurons in the trigeminal ganglia are highly sensitive to innocuous and noxious cooling (Lemon et al. 2016; Yarmolinsky et al. 2016; Leijon et al. 2019). Interestingly, while a subset of trigeminal

ganglia neurons is also sensitive to noxious heat, comparably fewer cells respond to innocuous warming (Yarmolinsky et al. 2016; Leijon et al. 2019). In rodents, neurons in the trigeminal ganglia activate second-order trigeminal neurons that project to the PBN—a brain region that is also part of the ascending gustatory pathway (PBN receives taste inputs from the nucleus of the solitary tract). A recent study has discovered that some trigeminal inputs supplying craniofacial somatosensation reach the same PBN neurons receiving gustatory inputs (Li and Lemon 2019). It is important to note that these trigeminal inputs reached PBN neurons that display sensitivity to aversive oral temperatures and tastes, highlighting the putative role of the PBN in processing and relaying multimodal intraoral sensory information, including gustatory, nociceptive, and thermal stimuli (Li et al. 2022). Thermal stimulation inside the mouth can also recruit taste-sensitive nerves. On the one hand, temperature can influence the peripheral taste-sensitive neurons in presence of gustatory stimuli via the warmth-activated transient receptor potential (TRP) melastatin 5 (TRPM5) cation channel, which is involved with GPCR-mediated transduction cascades for sweet, umami, and bitter taste stimuli (Zhang et al. 2003; Talavera et al. 2005), and the thermal-sensitive epithelial sodium channels (ENaCs), which are involved with sodium taste transduction (Askwith et al. 2001). On the other hand, temperature can influence the peripheral taste-sensitive neurons even in the absence of taste—a condition that is more relevant to the data presented in our study. Experimental evidence has indicated that a subset of chorda tympani neurons that do not respond to gustatory stimuli can be activated by cold fluid applied to the tip of the tongue (Yokota and Bradley 2016, 2017). In addition, electrophysiological recordings of chorda tympani nerves in taste-deficient mice have revealed oral thermal responses (Finger et al. 2005). Future studies combining cell-type, molecular, and circuit manipulation approaches will be key to unraveling more details of the oral thermal pathway.

### A "taste" of things to come

In the past 3 decades, multiple studies have shed important light on the taste responses of GC neurons in awake rodents (Samuelsen and Vincis 2021). Extracellular recordings and 2-photon experiments have extensively and convincingly described both the temporal and spatial profile of taste-evoked activity. For example, electrophysiological data have highlighted the importance of hundreds of milliseconds- and seconds-long temporal dynamics of taste-evoked spiking activity (Katz et al. 2001; Gutierrez et al. 2010; Neese et al. 2022), while imaging experiments have revealed the lack of chemotopic organization of these responses (Chen et al. 2021) [but see also Chen et al. (2011) and Fletcher et al. (2017) for in vivo data]. However, these results originated from studies in which taste stimuli were experienced at a single temperature. While such an approach has shaped our understanding of cortical taste processing, it provides only a partial picture of the functional features of the GC. It is a common experience that temperature is a cue relevant to food preference, and multiple studies have shown temperature's influence on taste perception (Moskowitz 1973; Bartoshuk et al. 1982; Green and Frankmann 1987; Torregrossa et al. 2012). In addition, our results indicate that GC activity is strongly modulated by oral fluid temperature and that gustatory and thermal inputs can converge on a subset of broadly tuned taste-selective neurons. For all of these reasons, one may wonder whether GC taste tuning, as well as the temporal and spatial properties of taste responses, are altered by the temperature of the stimulus and to what extent. Future experiments will examine the GC functional organization of chemosensory gustatory responses with respect to temperature–taste integration.

## Acknowledgments

The authors would like to acknowledge Dr. Chris Lemon, Dr. Richard Bertram, and the members of the Vincis laboratory for their feedback and insightful comments. They also thank Fred Fletcher and Te Tang for their excellent technical assistance. A portion of these data were presented in abstract form at the 2023 meeting of the Association for Chemoreception Sciences, Bonita Springs, FL.

## Author contributions

CGB and RV designed research; CGB and KEO performed research; CGB, KEO, CN, and RV analyzed data; RV wrote the first draft of the paper; KEO, CGB, and RV edited the paper; RV wrote the paper.

## Funding

This work was supported by funding from the National Institute of Deafness and Other Communication Disorders (NIDCD) of the National Institutes of Health (NIH), grant R01DC019326, and National Science Foundation (NSF), grant DMS 2324962 to RV, as well as by NIH-NIDCD grant T32 DC000044 to CGB.

## Conflict of interest statement

None declared.

## Data availability

Zeonodo (data) and GitHub (code to reproduce figures and stats) accession numbers will be made available after acceptance.

## References

Accolla R, Bathellier B, Petersen CC, Carleton A. Differential spatial representation of taste modalities in the rat gustatory cortex. J Neurosci. 2007:27:1396–1404.

Allchorne AJ, Broom DC, Woolf CJ. Detection of cold pain, cold allodynia and cold hyperalgesia in freely behaving rats. Mol Pain. 2005:1:1744–8069.

Arieli E, Gerbi R, Shein-Idelson M, Moran A. Temporally-precise basolateral amygdala activation is required for the formation of taste memories in gustatory cortex. J Physiol. 2020:598:5505–5522.

Askwith CC, Benson CJ, Welsh MJ, Snyder PM. Deg/enac ion channels involved in sensory transduction are modulated by cold temperature. Proc Natl Acad Sci USA. 2001:98:6459–6463.

Bartoshuk L, Rennert K, Rodin J, Stevens J. Effects of temperature on the perceived sweetness of sucrose. Physiol Behav 1982:28:905–910.

Baumer-Harrison C, Raymond MA, Myers TA, Sussman KM, Rynberg ST, Ugartechea AP, Lauterbach D, Mast TG, Breza JM. Optogenetic stimulation of type i gad65+ cells in taste buds activates gustatory

neurons and drives appetitive licking behavior in sodium-depleted mice. J Neurosci. 2020:40:7795–7810.
Beukema P, Cecil KL, Peterson E, Mann VR, Matsushita M, Takashima Y, Navlakha S, Barth AL. Trpm8-mediated somatosensation in mouse neocortex. J Comp Neurol. 2018:526:1444–1456.
Bouaichi CG, Vincis R. Cortical processing of chemosensory and hedonic features of taste in active licking mice. J Neurophysiol. 2020:123:1995–2009.
Breza JM, Nikonov AA, Contreras RJ. Response latency to lingual taste stimulation distinguishes neuron types within the geniculate ganglion. J Neurophysiol. 2010:103:1771–1784.
Buccino AP, Hurwitz CL, Garcia S, Magland J, Siegle JH, Hurwitz R, Hennig MH. Spikeinterface, a unified framework for spike sorting. Elife 2020:9:e61834.
Cerf-Ducastel B, Van de Moortele PF, MacLeod P, Le Bihan D, Faurion A. Interaction of gustatory and lingual somatosensory perceptions at the cortical level in the human: a functional magnetic resonance imaging study. Chem Senses. 2001:26:371–383.
Chen K, Kogan JF, Fontanini A. Spatially distributed representation of taste quality in the gustatory insular cortex of behaving mice. Curr Biol. 2021:31:247–256.e4.
Chen X, Gabitto M, Peng Y, Ryba NJ, Zuker CS. A gustotopic map of taste qualities in the mammalian brain. Science. 2011:333:1262–1266.
De Araujo IE, Kringelbach ML, Rolls ET, McGlone F. Human cortical responses to water in the mouth, and the effects of thirst. J Neurophysiol. 2003:90:1865–1876.
Dikecligil GN, Graham DM, Park IM, Fontanini A. Layer-and cell type-specific response properties of gustatory cortex neurons in awake mice. J Neurosci. 2020:40:9676–9691.
Dotson CD, Colbert CL, Garcea M, Smith JC, Spector AC. The consequences of gustatory deafferentation on body mass and feeding patterns in the rat. Am J Physiol Regul Integr Comp Physiol. 2012:303:R611–R623.
Finger TE, Danilova V, Barrows J, Bartel DL, Vigers AJ, Stone L, Hellekant G, Kinnamon SC. Atp signaling is crucial for communication from taste buds to gustatory nerves. Science. 2005:310:1495–1499.
Fletcher ML, Ogg MC, Lu L, Ogg RJ, Boughter JD. Overlapping representation of primary tastes in a defined region of the gustatory cortex. J Neurosci. 2017:37:7595–7605.
Green BG, Frankmann SP. The effect of cooling the tongue on the perceived intensity of taste. Chem Senses. 1987:12:609–619.
Guest S, Grabenhorst F, Essick G, Chen Y, Young M, McGlone F, de Araujo I, Rolls ET. Human cortical representation of oral temperature. Physiol Behav 2007:92:975–984.
Gutierrez R, Simon SA, Nicolelis MA. Licking-induced synchrony in the taste–reward circuit improves cue discrimination during learning. J Neurosci. 2010:30:287–303.
Jezzini A, Mazzucato L, La Camera G, Fontanini A. Processing of hedonic and chemosensory features of taste in medial prefrontal and insular networks. J Neurosci. 2013:33:18966–18978.
Katz DB, Simon S, Nicolelis MA. Dynamic and multimodal responses of gustatory cortical neurons in awake rats. J Neurosci. 2001:21:4478–4489.
Kay KE, Martin LE, James KF, Haygood SM, Torregrossa AM. Temperature is sufficient to condition a flavor preference for a cold-paired solution in rats. Chem Senses. 2020:45:563–572.
Kemp SE, Beauchamp GK. Flavor modification by sodium chloride and monosodium glutamate. J Food Sci. 1994:59:682–686.
Kosar E, Grill HJ, Norgren R. Gustatory cortex in the rat. I. Physiological properties and cytoarchitecture. Brain Res. 1986:379:329–341.
Leijon SC, Neves AF, Breza JM, Simon SA, Chaudhari N, Roper SD. Oral thermosensing by murine trigeminal neurons: modulation by capsaicin, menthol and mustard oil. J Physiol. 2019:597:2045–2061.
Lemon CH. Tasting temperature: neural and behavioral responses to thermal stimulation of oral mucosa. Curr Opin Physiol 2021:20:16–22.
Lemon CH, Kang Y, Li J. Separate functions for responses to oral temperature in thermo-gustatory and trigeminal neurons. Chem Senses. 2016:41:457–471.
Levitan D, Lin JY, Wachutka J, Mukherjee N, Nelson SB, Katz DB. Single and population coding of taste in the gustatory cortex of awake mice. J Neurophysiol. 2019:122:1342–1356.
Li J, Ali MSS, Lemon CH. Trpv1-lineage somatosensory fibers communicate with taste neurons in the mouse parabrachial nucleus. J Neurosci. 2022:42:1719–1737.
Li J, Lemon CH. Mouse parabrachial neurons signal a relationship between bitter taste and nociceptive stimuli. J Neurosci. 2019:39:1631–1648.
Liu H, Fontanini A. State dependency of chemosensory coding in the gustatory thalamus (vpmpc) of alert rats. J Neurosci. 2015:35:15479–15491.
Maier JX. Single-neuron responses to intraoral delivery of odor solutions in primary olfactory and gustatory cortex. J Neurophysiol. 2017:117:1293–1304.
Moskowitz HR. Effects of solution temperature on taste intensity in humans. Physiol Behav 1973:10:289–292.
Mukherjee N, Wachutka J, Katz DB. Impact of precisely-timed inhibition of gustatory cortex on taste behavior depends on single-trial ensemble dynamics. Elife 2019:8:e45968.
Nakamura K, Norgren R. Gustatory responses of neurons in the nucleus of the solitary tract of behaving rats. J Neurophysiol. 1991:66:1232–1248.
Neese C, Bouaichi CG, Needham T, Bauer M, Bertram R, Vincis R. Active licking shapes cortical taste coding. J Neurosci. 2022:42:8658–8669.
Pachitariu M, Steinmetz NA, Kadir SN, Carandini M, Harris KD. Fast and accurate spike sorting of high-channel count probes with kilosort. Adv Neural Inform Process Syst. 2016:29.
Piette CE, Baez-Santiago MA, Reid EE, Katz DB, Moran A. Inactivation of basolateral amygdala specifically eliminates palatability-related information in cortical sensory responses. J Neurosci. 2012:32:9981–9991.
Rainer G, Asaad WF, Miller EK. Selective representation of relevant information by neurons in the primate prefrontal cortex. Nature. 1998:393:577–579.
Rosen AM, Roussin AT, Di Lorenzo PM. Water as an independent taste modality. Front Neurosci. 2010:4:175.
Roussin AT, D'Agostino AE, Fooden AM, Victor JD, Di Lorenzo PM. Taste coding in the nucleus of the solitary tract of the awake, freely licking rat. J Neurosci. 2012:32:10494–10506.
Rudenga K, Green B, Nachtigal D, Small D. Evidence for an integrated oral sensory module in the human anterior ventral insula. Chem Senses. 2010:35:693–703.
Samuelsen CL, Fontanini A. Processing of intraoral olfactory and gustatory signals in the gustatory cortex of awake rats. J Neurosci. 2017:37:244–257.
Samuelsen CL, Gardner MP, Fontanini A. Thalamic contribution to cortical processing of taste and expectation. J Neurosci. 2013:33:1815–1827.
Samuelsen CL, Vincis R. Cortical hub for flavor sensation in rodents. Front Syst Neurosci. 2021:15:772286.
Schier LA, Spector AC. The functional and neurobiological properties of bad taste. Physiol Rev. 2019:99:605–663.
Small DM. Flavor is in the brain. Physiol Behav 2012:107:540–552.
Small DM, Voss J, Mak YE, Simmons KB, Parrish T, Gitelman D. Experience-dependent neural integration of taste and smell in the human brain. J Neurophysiol. 2004:92:1892–1903.
Spector AC, Travers SP. The representation of taste quality in the mammalian nervous system. Behav Cogn Neurosci Rev. 2005:4:143–191.
Stapleton JR, Lavine ML, Wolpert RL, Nicolelis MA, Simon SA. Rapid taste responses in the gustatory cortex during licking. J Neurosci. 2006:26:4126–4138.
Suzuki R, Hunt SP, Dickenson AH. The coding of noxious mechanical and thermal stimuli of deep dorsal horn neurones is attenuated in NK1 knockout mice. Neuropharmacology. 2003:45:1093–1100.
Talavera K, Yasumatsu K, Voets T, Droogmans G, Shigemura N, Ninomiya Y, Margolskee RF, Nilius B. Heat activation of

TRPM5 underlies thermal sensitivity of sweet taste. Nature. 2005:438:1022–1025.
Torregrossa AM, Bales MB, Breza JM, Houpt TA, Smith JC, Contreras RJ. Water restriction and fluid temperature alter preference for water and sucrose solutions. Chem Senses. 2012:37:279–292.
Travers SP, Kalyanasundar B, Breza J, Houser G, Klimovich C, Travers J. Characteristics and impact of the rNST GABA network on neural and behavioral taste responses. Eneuro 2022:9.
Verhagen JV, Kadohisa M, Rolls ET. Primate insular/opercular taste cortex: neuronal representations of the viscosity, fat texture, grittiness, temperature, and taste of foods. J Neurophysiol. 2004:92:1685–1699.
Vestergaard M, Carta M, Güney G, Poulet J. The cellular coding of temperature in the mammalian cortex. Nature. 2023:614:725–731.
Vincis R, Chen K, Czarnecki L, Chen J, Fontanini A. Dynamic representation of taste-related decisions in the gustatory insular cortex of mice. Curr Biol. 2020:30:1834–1844.e5.
Vincis R, Fontanini A. Associative learning changes cross-modal representations in the gustatory cortex. Elife 2016a:5:e16420.
Vincis R, Fontanini A. A gustocentric perspective to understanding primary sensory cortices. Curr Opin Neurobiol. 2016b:40:118–124.
Vincis R, Fontanini A. Central taste anatomy and physiology. Handb Clin Neurol 2019:164:187–204.
Wang L, Zhang Z, Chen J, Manyande A, Haddad R, Liu Q, Xu F. Cell-type-specific whole-brain direct inputs to the anterior and posterior piriform cortex. Front Neural Circuits. 2020:14:4.
Wilson DM, Lemon CH. Modulation of central gustatory coding by temperature. J Neurophysiol. 2013:110:1117–1129.
Yamamoto T, Yuyama N, Kawamura Y. Cortical neurons responding to tactile, thermal and taste stimulations of the rat's tongue. Brain Res. 1981:221:202–206.
Yarmolinsky DA, Peng Y, Pogorzala LA, Rutlin M, Hoon MA, Zuker CS. Coding and plasticity in the mammalian thermosensory system. Neuron. 2016:92:1079–1092.
Yokota Y, Bradley RM. Receptive field size, chemical and thermal responses, and fiber conduction velocity of rat chorda tympani geniculate ganglion neurons. J Neurophysiol. 2016:115:3062–3072.
Yokota Y, Bradley RM. Geniculate ganglion neurons are multimodal and variable in receptive field characteristics. Neuroscience. 2017:367:147–158.
Yoshida T, Katz DB. Control of prestimulus activity related to improved sensory coding within a discrimination task. J Neurosci. 2011:31:4101–4112.
Zhang Y, Hoon MA, Chandrashekar J, Mueller KL, Cook B, Wu D, Zuker CS, Ryba NJ. Coding of sweet, bitter, and umami tastes: different receptor cells sharing similar signaling pathways. Cell. 2003:112:293–301.
Zocchi D, Wennemuth G, Oka Y. The cellular mechanism for water detection in the mammalian taste system. Nat Neurosci. 2017:20:927–933.